Pergamon

International Journal of Plasticity, Vol. 10, No. 7, pp. 761–793, 1994

0749-6419/94 $6.00 + .00

0749-6419(94)00023-9

CRACK PROPAGATION IN POROUS HARDENING METALS

ENRICO RADI and DAVIDE BIGONI

University of Bologna

Abstract—Steady-state and quasi-static rectilinear crack propagation is analyzed in porous elastoplastic solids obeying the Gurson yield condition and flow-law. Both plane strain and plane stress conditions are considered under Mode I and Mode II loading conditions. The asymptotic crack-tip fields are obtained with reference to the incremental small strain theory in the case of linear isotropic hardening behavior of the matrix material. The porosity of the material is assumed constant, therefore the elastoplastic constitutive operator results in being self-adjoint. Elastic unloading and plastic reloading on crack flanks are taken into account.

1. INTRODUCTION

The determination of asymptotic stress and strain fields in the plastic zone near a crack-tip is fundamental in the understanding of crack propagation mechanisms. The case of a steadily propagating crack in the framework of the J_2-flow theory with linear hardening was initially developed by AMAZIGO and HUTCHINSON [1977], under the hypothesis of HRR singularity in the fields ahead of the crack-tip (HUTCHINSON [1968a,1968b]; RICE & ROSENGREN [1968]). Later, the problem was considered by PONTE CASTAÑEDA [1987], who accounted for plastic reloading on crack flanks, by ACHENBACH *et al.* [1981] and ÖSTLUND and GUDMUNDSON [1988], who investigated dynamic propagation.

In recent papers (BIGONI & RADI [1993] and RADI & BIGONI [1993]), the authors analyzed crack propagation in elastoplastic pressure-sensitive solids with associative and nonassociative flow-rules, employing a constitutive model based on the Drucker–Prager yield condition, namely, the small strain version of the RUDNICKI and RICE [1975] model. This constitutive model can be useful in a rough modelling of many materials of engineering importance, for example, ceramics, rocks, concrete, metals showing the S-D effect and porous metals. Moreover, in RADI and BIGONI [1993], a first effort was expended in the direction of the analysis of nonassociativity effects on crack propagation.

Porous metals and particulate-reinforced metal matrix composites are known to exhibit pressure sensitivity and volumetric changes during plastic flow processes. Of this behavior, the Drucker–Prager model with isotropic hardening gives only a first approximation (TVERGAARD [1990]). More precise modelling can be achieved by employing the elastoplastic model proposed by GURSON [1977a,1977b] and subsequently modified by TVERGAARD [1981,1982] and TVERGAARD and NEEDLEMAN [1984]. The Gurson model originated from micromechanical considerations in which the voids were assumed to be spherical and the matrix material rigid-plastic. Gurson extended the model to isotropic hardening and later MEAR and HUTCHINSON [1985], and TVERGAARD [1987] introduced kinematic hardening. This model was investigated from many points of view. Strain

localization into narrow planar bands was analysed by NEEDLEMAN and RICE [1978], YAMAMOTO [1978], SAJE *et al.* [1982], OHNO and HUTCHINSON [1984], MEAR and HUTCHINSON [1985], and TVERGAARD and VAN DER GIESSEN [1991]. Surface instabilities were considered by TVERGAARD [1982]. However, fracture mechanics, that was thoroughly investigated via f.e. methods by ARAVAS and MCMEEKING [1985], AOKI *et al.* [1987], NEEDLEMAN and TVERGAARD [1987], JAGOTA *et al.* [1987], TVERGAARD and NEEDLEMAN [1992], AOKI *et al.* [1992], was never analyzed from the point of view of asymptotic analysis until quite recently. In fact, the only contribution in this direction was given by DRUGAN and MIAO [1992], in the case of a stationary crack in plane strain and Mode I conditions, under the hypotheses of constant porosity and perfect plastic behavior of the matrix material.

This article concerns itself with an asymptotic analysis of steady-state crack propagation in an elastoplastic material obeying the Gurson yield function and flow-law. As in DRUGAN and MIAO [1992], the hypothesis is introduced of constant porosity. It should be noted that the behavior of incompletely sintered and previously deformed metals can be modelled with this assumption. As noted by HUTCHINSON [1983a], the method of asymptotic analysis is valid in an annular zone close to the crack-tip, which is small if compared to the size of the plastic sector. The internal radius is determined by the magnitude of the zone where micro-inhomogeneities, cavitation, and finite deformation effects dominate. Therefore, the assumption of constant porosity can be appropriate in the range of applicability of asymptotic analysis. In any case, the inclusion of a nucleation law for the porosity not only complicates the analytical computations, but may yield a nonadjoint elastoplastic operator. This circumstance, as discussed in RADI and BIGONI [1993], may cause a loss of ellipticity of the PDEs governing the problem, with possibility of the appearance of stress discontinuities.

Mode II loading condition has been explored in elastoplastic materials by AMAZIGO and HUTCHINSON [1977], PONTE CASTAÑEDA [1987], ACHENBACH *et al.* [1981], and ÖSTLUND and GUDMUNDSON [1988]. These investigations are restricted to the case of J_2-flow theory only. Therefore, for pressure-sensitive solids, the problem is almost unexplored. This may be due to the fact that the different behavior in tension and compression of many yield criteria for pressure-sensitive solids (e.g. the Drucker–Prager, Schleicher, Coulomb–Mohr, and Elliptic yield surfaces, Fig. 2) breaks the symmetry of the Mode II conditions. There exist, however, yield criteria that are pressure-sensitive but insensitive to the sign of the stress. A typical example of this behavior is represented by the BELTRAMI [1885] yield condition. This criterion is represented by an ellipsoid centred at the origin of the Haigh–Westergaard stress space, with the axis of revolution coincident with the hydrostatic axis. The Gurson yield criterion, which has the meridian section shown in Fig. 1, is another example of pressure-sensitive criterion independent of the sign of the stress. In any case, the type of yield function is not the only source of breaking the Mode II symmetry; in fact, all plasticity rules must be insensitive to the sign of the stress. In the case of the Gurson model (GURSON [1977a,1977b]), the evolution law of the porosity (see TVERGAARD [1981,1982]) changes with the sign of the stress. However, in the particular case of constant porosity and isotropic hardening of the matrix material, Mode II symmetry is preserved.

Ductile Mode II crack growth in extremely rare in real application of civil and marine structures. However, Mode II ductile crack growth occurs on interface problem in electronic type materials, and its analysis is the basis for mixed mode crack propagation problems. As far as the authors are aware, asymptotic analyses are not available for Mode II propagation in porous elastoplastic materials obeying the Gurson model. In this

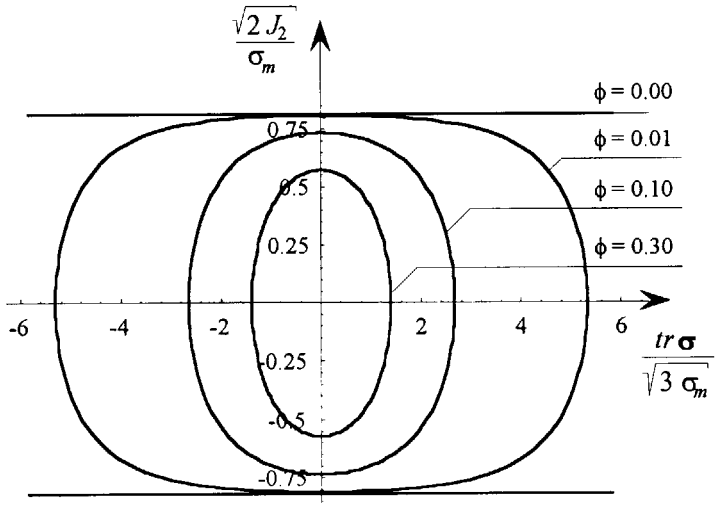

Fig. 1. Meridian section of the Gurson yield surface.

research direction, the only contribution concerns F.E. analyses. In particular, the investigation performed by AOKI *et al.* [1987] is more closely related to the result that will be presented.

The asymptotic problem is solved by using the procedure introduced by PONTE CASTAÑEDA [1987], which allows to take into account elastic unloading in the crack wake and plastic reloading on crack flanks. Results are given for the near tip stress and velocity fields as functions of matrix hardening and porosity parameters. When the porosity is set equal to zero, the *J_2-flow theory* is recovered and the results reduce to those by PONTE CASTAÑEDA [1987]. Both the conditions of plane strain and plane stress are analysed in Mode I and Mode II loading conditions. The obtained results emphasize the

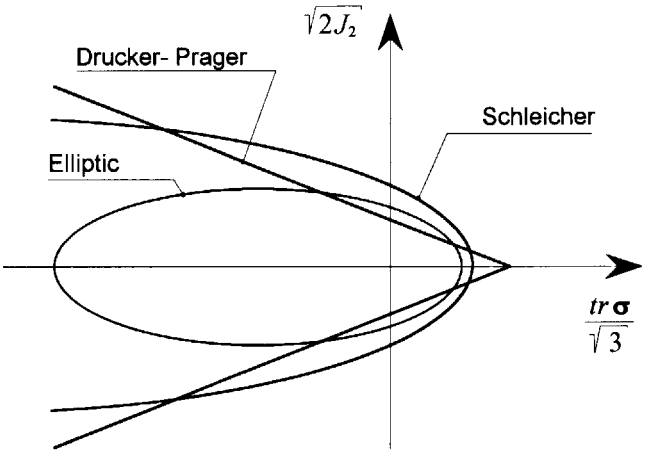

Fig. 2. Meridian sections of the Drucker–Prager, Schleicher, and Elliptic yield surfaces.

effects of the porosity on the asymptotic fields. Due to the high value of mean stress, this effect is more pronounced under plane strain and Mode I loading, rather than under plane stress or Mode II conditions. This circumstance agrees with the results obtained for crack propagation in materials obeying the Drucker–Prager model (BIGONI & RADI [1993]; RADI & BIGONI [1993]). However, the Gurson yield surface has curved meridian sections and is closed and smooth at every point (included intersections with the hydrostatic axis; see Fig. 1). As a consequence, the stress states near crack-tip are different from those obtained when the Drucker–Prager model is adopted. In the case of the Gurson model in Mode I plane strain, for instance, the stress state ahead of the crack-tip does not tend to the hydrostatic state of stress. Moreover, by increasing the porosity, the radial stress component tends to coincide with the out-of-plane stress component, in the whole plastic sector ahead of the crack tip.

Finally, it is worth mentioning that the obtained solutions correspond to *continuous* stress and velocity fields. This circumstance agrees with the argument proved by DRUGAN and RICE [1984], which does not cover the condition of perfect plastic behavior. Therefore, the stress jumps evidenced in the solution by DRUGAN and MIAO [1992] are consistent. These jumps occur for a "critical" value of porosity and fit coherently with the solution proposed in this article. In fact, for low hardening behavior of the matrix material, the obtained stress fields show a definite change around the mentioned critical value of porosity.

This article is organized as follows. In Section II, the Gurson model is briefly reviewed, and in Section III the general equations, which govern the propagation problem, are derived. Sections IV and V address the plane strain and plane stress problems for Mode I loading. Mode II loading is examined in Sections VI and VII. In these sections, stress and velocity fields near crack-tip are obtained by performing an asymptotic analysis, and the results are presented and elucidated.

II. CONSTITUTIVE MODEL

The yield condition corresponding to the Gurson model, in the version modified by TVERGAARD [1981,1982], is:

$$f(\boldsymbol{\sigma}, \sigma_m) = \frac{3J_2}{\sigma_m^2} + 2q_1\phi \cosh\left(\frac{q_2}{2}\frac{\operatorname{tr}\boldsymbol{\sigma}}{\sigma_m}\right) - 1 - (q_1\phi)^2 = 0, \tag{1}$$

where $\boldsymbol{\sigma}$ denotes the (macroscopic) stress tensor, J_2 the second invariant of deviatoric (macroscopic) stress, σ_m is an equivalent tensile flow stress representing the actual microscopic stress-state in the matrix material. Moreover, q_1 and q_2 are the parameters introduced by TVERGAARD [1981,1982] and ϕ is the volume fraction of voids. Let Φ denote the product $q_1\phi$. In the following, the void volume fraction ϕ will be assumed constant, as in DRUGAN and MIAO [1992]. The associative plastic flow law is:

$$\dot{\boldsymbol{\varepsilon}}^{\mathrm{p}} = \Lambda \mathbf{Q}; \tag{2}$$

in eqn (2) Λ is the (nonnegative) plastic multiplier and $\mathbf{Q}$ is the gradient of the yield function (1):

$$\mathbf{Q} = \frac{\sigma_m}{2}\frac{\partial f}{\partial \boldsymbol{\sigma}} = \alpha\mathbf{I} + \frac{3}{2\sigma_m}\mathbf{S}, \tag{3}$$

where $\mathbf{S}$ denotes the deviatoric (macroscopic) stress, and the scalar α has the expression:

$$\alpha = \Phi \frac{q_2}{2} \sinh\left(\frac{q_2}{2} \frac{\operatorname{tr} \boldsymbol{\sigma}}{\sigma_m}\right). \tag{4}$$

In the case of isotropic hardening, the rate of equivalent plastic work in the matrix material is assumed equal to the macroscopic rate of plastic work:

$$\boldsymbol{\sigma} \cdot \dot{\boldsymbol{\varepsilon}}^{\mathrm{p}} = (1 - \phi)\sigma_m \dot{\varepsilon}_m^{\mathrm{p}}, \tag{5}$$

where $\dot{\varepsilon}_m^{\mathrm{p}}$ is the effective plastic strain rate (work-conjugate with σ_m), representing the microscopic strain-state in the matrix material. Assuming for the matrix an elastoplastic constitutive relationship based on the *J_2-flow theory* with linear hardening, the following relationship between the equivalent stress and the effective plastic strain rate holds true:

$$\dot{\sigma}_m = 3\mathrm{H}_m \dot{\varepsilon}_m^{\mathrm{p}}, \tag{6}$$

where H_m is the hardening modulus of the matrix material, which depends on the ratio α_{G} between the tangential shear modulus G_{t} and the elastic shear modulus G of the matrix material:

$$\mathrm{H}_m = \frac{\alpha_{\mathrm{G}}}{1 - \alpha_{\mathrm{G}}} \mathrm{G}. \tag{7}$$

The relation governing the evolution of σ_m follows from (5), by using (6), (2), and (3) in the form:

$$\dot{\sigma}_m = \Lambda \frac{3\mathrm{H}_m}{(1 - \phi)\sigma_m} \mathbf{Q} \cdot \boldsymbol{\sigma}. \tag{8}$$

The value of the plastic multiplier is obtained by imposing Prager consistency:

$$\Lambda = \frac{\langle \mathbf{Q} \cdot \dot{\boldsymbol{\sigma}} \rangle}{\mathrm{H}}, \tag{9}$$

where $\langle\ \rangle$ denotes the McAulay brackets, i.e. the operator $\mathbb{R} \to \mathbb{R}^+ \cup \{0\}$: $\forall \chi \in \mathbb{R}$, $\langle \chi \rangle = \mathrm{Sup}\{\chi, 0\}$, and the macroscopic hardening modulus H is given by:

$$\mathrm{H} = \frac{3\mathrm{H}_m}{(1 - \phi)\sigma_m^2} (\mathbf{Q} \cdot \boldsymbol{\sigma})^2. \tag{10}$$

It should be noted that a positive hardening modulus of the matrix material implies a positive hardening behavior of the porous (homogenized) material ($\mathrm{H}_m > 0 \Rightarrow \mathrm{H} > 0$).

Assuming isotropic elastic behavior, the elastoplastic incremental constitutive equations, relating the stress rate $\dot{\boldsymbol{\sigma}}$ to the velocity of deformation $\dot{\boldsymbol{\varepsilon}}$, can finally be obtained in the standard form:

$$\dot{\boldsymbol{\varepsilon}} = \frac{1}{2G}\left[\dot{\boldsymbol{\sigma}} - \frac{\nu}{1+\nu}(\operatorname{tr}\dot{\boldsymbol{\sigma}})\mathbf{I}\right] + \Lambda\mathbf{Q}, \tag{11}$$

where ν is the Poisson ratio.

It is worth noting that σ_m plays the role of a hardening scalar parameter and that the assumption of constant porosity implies that void nucleation is absent and thus yields a symmetric elastoplastic operator. Moreover, the analogies between the present and the Drucker–Prager models should also be noted. In fact, the constitutive equation (11) with $\mathbf{Q}$ given by (3) differs from the associative Drucker–Prager model (see, e.g. BIGONI & RADI [1993]) for the particular evolution laws of H, α, and, of course, for the yield function. In particular, the Gurson yield surface is smooth in correspondence of the hydrostatic axis and is closed in stress space. These circumstances yield different behavior with respect to the Drucker–Prager plasticity. It may be interesting to show that for radial stress paths, the constitutive equations (8–11) exhibit constant hardening. To this purpose, let us assume:

$$\boldsymbol{\sigma} = \beta\boldsymbol{\xi}, \qquad \text{consequently} \qquad \dot{\boldsymbol{\sigma}} = \dot{\beta}\boldsymbol{\xi}, \tag{12}$$

in which the constant-unit norm tensor $\boldsymbol{\xi}$ fixes the direction of $\boldsymbol{\sigma}$ and $\dot{\boldsymbol{\sigma}}$ in the stress space and $\dot{\beta}$ specifies the norm increment. A substitution of eqns (10) and (9) into eqn (8) gives the following identity, which holds true during plastic flow:

$$\frac{\dot{\sigma}_m}{\sigma_m} = \frac{\mathbf{Q}\cdot\dot{\boldsymbol{\sigma}}}{\mathbf{Q}\cdot\boldsymbol{\sigma}}. \tag{13}$$

Conditions (12) may be substituted in eqn (13) and integrated to give:

$$\sigma_m = k\beta, \tag{14}$$

where k must be obtained as the positive solution of the following equation:

$$\frac{3\operatorname{dev}\boldsymbol{\xi}\cdot\operatorname{dev}\boldsymbol{\xi}}{2k^2} + 2\Phi\cosh\left(\frac{q_2}{2}\frac{\operatorname{tr}\boldsymbol{\xi}}{k}\right) - 1 - \Phi^2 = 0, \tag{15}$$

where the symbol dev denotes the deviatoric part of a tensor. The substitution of (12) and (14) into (10) yields:

$$\mathrm{H} = \frac{3\mathrm{H}_m}{(1-\phi)k^2}(\mathbf{Q}\cdot\boldsymbol{\xi})^2, \tag{16}$$

where $\mathbf{Q}$ is obtained from (3) in the form:

$$\mathbf{Q} = \Phi\frac{q_2}{2}\sinh\left(\frac{q_2}{2}\frac{\operatorname{tr}\boldsymbol{\xi}}{k}\right)\mathbf{I} + \frac{3}{2k}\operatorname{dev}\boldsymbol{\xi}. \tag{17}$$

From (16) and (17) it is easily concluded that, for the considered constitutive model, *the hardening modulus* H *is constant during radial stress paths emanating from the origin of the stress space.* However, the stress path of near crack-tip particles is not radial, and thus the hardening modulus changes during crack-tip loading.

III. CRACK PROPAGATION PROBLEM

In the problem under consideration, a rectilinear crack is supposed to propagate at constant velocity in an infinite medium of elastoplastic material, obeying the constitutive rules described in the previous section. In this propagation problem, elastic unloading zones are involved as sketched in Fig. 3. Therefore, a full incremental theory of elastoplasticity has to be employed. This will be done on the basis of the method proposed by PONTE CASTAÑEDA [1987].

A cylindrical coordinate system (r,ϑ,x_3) is employed with the origin attached to the moving crack-tip, which is propagating in the $\vartheta = 0$ direction. The x_3-axis is assumed along the direction of zero stress or strain. For this choice of the reference frame, the steady-state propagation condition implies:

$$(\dot{\ }) = \frac{c}{r}\,[(\ )_{,\vartheta}\sin\vartheta - r(\ )_{,r}\cos\vartheta\,], \tag{18}$$

where c denotes the (constant) crack-tip speed and the comma indicates differentiation. The kinematic compatibility conditions are:

$$\dot{\varepsilon}_{rr} = v_{r,r}, \qquad \dot{\varepsilon}_{\vartheta\vartheta} = (v_{\vartheta,\vartheta} + v_r)/r, \qquad \dot{\varepsilon}_{r\vartheta} = (rv_{\vartheta,r} + v_{r,\vartheta} - v_\vartheta)/(2r), \tag{19}$$

where v_i are the velocity components.

The problem is formulated by taking the stress and the two in-plane velocity components as unknown functions. The equilibrium equations in cylindrical coordinates are:

$$(r\sigma_{rr})_{,r} + \sigma_{r\vartheta,\vartheta} - \sigma_{\vartheta\vartheta} = 0, \qquad (r\sigma_{r\vartheta})_{,r} + \sigma_{\vartheta\vartheta,\vartheta} + \sigma_{r\vartheta} = 0. \tag{20}$$

In cylindrical coordinates, the elastoplastic relationship (11), may be written as

$$\begin{aligned}
\dot{\varepsilon}_{rr} &= [\dot{\sigma}_{rr} - \nu(\dot{\sigma}_{\vartheta\vartheta} + \dot{\sigma}_{33})]/E + \Lambda Q_{rr},\\
\dot{\varepsilon}_{\vartheta\vartheta} &= [\dot{\sigma}_{\vartheta\vartheta} - \nu(\dot{\sigma}_{rr} + \dot{\sigma}_{33})]/E + \Lambda Q_{\vartheta\vartheta},\\
\dot{\varepsilon}_{33} &= [\dot{\sigma}_{33} - \nu(\dot{\sigma}_{rr} + \dot{\sigma}_{\vartheta\vartheta})]/E + \Lambda Q_{33},\\
\dot{\varepsilon}_{r\vartheta} &= [(1+\nu)\dot{\sigma}_{r\vartheta}]/E + \Lambda Q_{r\vartheta},
\end{aligned} \tag{21}$$

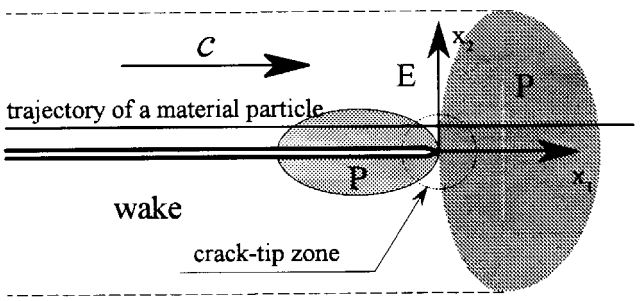

Fig. 3. Plastic zone near a propagating crack-tip.

where E is Young modulus and the components of the stress rate tensor are:

$$\dot{\sigma}_{r\vartheta} = \frac{c}{r}\left[(\sigma_{r\vartheta,\vartheta} + \sigma_{rr} - \sigma_{\vartheta\vartheta})\sin\vartheta - r\sigma_{r\vartheta,r}\cos\vartheta\right],$$

$$\dot{\sigma}_{rr} = \frac{c}{r}\left[(\sigma_{rr,\vartheta} - 2\sigma_{r\vartheta})\sin\vartheta - r\sigma_{rr,r}\cos\vartheta\right],$$

$$\dot{\sigma}_{\vartheta\vartheta} = \frac{c}{r}\left[(\sigma_{\vartheta\vartheta,\vartheta} + 2\sigma_{r\vartheta})\sin\vartheta - r\sigma_{\vartheta\vartheta,r}\cos\vartheta\right], \tag{22}$$

$$\dot{\sigma}_{33} = \begin{cases} 0 & \text{plane stress} \\ \dfrac{c}{r}\left(\sigma_{33,\vartheta}\sin\vartheta - r\sigma_{33,r}\cos\vartheta\right) & \text{plane strain.} \end{cases}$$

Equilibrium eqns (20) and constitutive eqns (21) form a system of first order PDEs, which governs the problem of the crack propagation. We look now for solutions in the HRR separable form (HUTCHINSON [1968a,1968b]; RICE & ROSENGREN [1968])

$$\begin{aligned} v_r(r,\vartheta) &= (c/s)\underline{r}^s y_1(\vartheta), & v_\vartheta(r,\vartheta) &= (c/s)\underline{r}^s y_2(\vartheta), \\ \sigma_{r\vartheta}(r,\vartheta) &= E\underline{r}^s y_3(\vartheta), & \sigma_{rr}(r,\vartheta) &= E\underline{r}^s y_4(\vartheta), \\ \sigma_{\vartheta\vartheta}(r,\vartheta) &= E\underline{r}^s y_5(\vartheta), & \sigma_{33}(r,\vartheta) &= E\underline{r}^s y_6(\vartheta), \end{aligned} \tag{23}$$

where s is the fields singularity exponent and $\underline{r}$ denotes the nondimensional ratio between r and any characteristic dimension of the plastic zone. The solution can be determined except for an amplitude factor, as expected from asymptotic analysis of a homogeneous problem.

A representation similar to (23) is introduced for σ_m:

$$\sigma_m(r,\vartheta) = E\underline{r}^s y_m(\vartheta). \tag{24}$$

A substitution of (23) into the equilibrium eqns (20) yields the following expressions for y_3' and y_5':

$$y_3' = -(1+s)y_4 + y_5, \tag{25}$$

$$y_5' = -(2+s)y_3. \tag{26}$$

When the representations (23) are substituted into the compatibility conditions (19) and the steady-state condition (18) is employed, the strain rates may be written as:

$$\begin{aligned} \dot{\varepsilon}_{rr} &= (c/r)\underline{r}^s y_1, \\ \dot{\varepsilon}_{\vartheta\vartheta} &= (c/r)\underline{r}^s/s(y_2' + y_1), \\ \dot{\varepsilon}_{r\vartheta} &= (c/r)\underline{r}^s/(2s)\left[y_1' - (1-s)y_2\right]. \end{aligned} \tag{27}$$

Similarly, when (23) are substituted into (22), the dimensionless stress rate tensor, defined as:

$$\boldsymbol{\Sigma} = \frac{\dot{\boldsymbol{\sigma}}}{(c/\mathrm{r})\mathrm{E}\underline{\mathrm{r}}^{s}}, \tag{28}$$

results in the following representation in terms of functions y_i.

$$\begin{aligned}
\Sigma_{\mathrm{r}\vartheta} &= -s(\mathrm{y}_4 \sin\vartheta + \mathrm{y}_3 \cos\vartheta),\\
\Sigma_{\mathrm{rr}} &= (\mathrm{y}_4' - 2\mathrm{y}_3)\sin\vartheta - s\mathrm{y}_4 \cos\vartheta,\\
\Sigma_{\vartheta\vartheta} &= -s(\mathrm{y}_3 \sin\vartheta + \mathrm{y}_5 \cos\vartheta),\\
\Sigma_{33} &= \begin{cases} 0 & \textit{plane stress},\\ \mathrm{y}_6' \sin\vartheta - s\mathrm{y}_6 \cos\vartheta & \textit{plane strain}. \end{cases}
\end{aligned} \tag{29}$$

It is worth noting that y_3' and y_5' do not appear in the expressions for $\Sigma_{\mathrm{r}\vartheta}$ and $\Sigma_{\vartheta\vartheta}$, since equilibrium eqns (25) and (26) have been used to get $(29_{1,3})$. Moreover, from representation (24) the dimensionless rate of σ_m results to be:

$$\Sigma_m = \frac{\dot{\sigma}_m}{(c/\mathrm{r})\mathrm{E}\underline{\mathrm{r}}^{s}} = \mathrm{y}_m' \sin\vartheta - s\mathrm{y}_m \cos\vartheta. \tag{30}$$

When the stress functions (23,24) are employed, the components of the yield function gradient (3) become:

$$\begin{aligned}
\mathrm{Q}_{\mathrm{rr}} &= \alpha + \frac{2\mathrm{y}_4 - \mathrm{y}_5 - \mathrm{y}_6}{2\mathrm{y}_m}, \qquad \mathrm{Q}_{\vartheta\vartheta} = \alpha + \frac{2\mathrm{y}_5 - \mathrm{y}_4 - \mathrm{y}_6}{2\mathrm{y}_m},\\
\mathrm{Q}_{33} &= \alpha + \frac{2\mathrm{y}_6 - \mathrm{y}_4 - \mathrm{y}_5}{2\mathrm{y}_m}, \qquad \mathrm{Q}_{\mathrm{r}\vartheta} = \frac{3\mathrm{y}_3}{2\mathrm{y}_m},
\end{aligned} \tag{31}$$

where:

$$\alpha = \Phi \frac{q_2}{2} \sinh\left[\frac{q_2}{2} \frac{(\mathrm{y}_4 + \mathrm{y}_5 + \mathrm{y}_6)}{\mathrm{y}_m}\right]. \tag{32}$$

A substitution of the expressions (22–24) and (27–32) into the incremental constitutive relationships (8) and (21), together with equilibrium eqns (25,26), yields the system of equations governing the near-tip stress and velocity fields. This system results in seven first order ODEs, whose unknown functions are the velocity and stress functions $\mathrm{y}_1(\vartheta), \mathrm{y}_2(\vartheta), \ldots, \mathrm{y}_6(\vartheta)$, and $\mathrm{y}_m(\vartheta)$. The unknown functions reduce to six in plane stress conditions ($\sigma_{33} = \mathrm{y}_6 = 0$). The system of first order ODEs may be cast in the following standard form:

$$\mathbf{y}'(\vartheta) = \mathbf{f}(\vartheta, \mathbf{y}(\vartheta), s), \tag{33}$$

where: $\mathbf{y}(\vartheta) = \{\mathrm{y}_1(\vartheta), \mathrm{y}_2(\vartheta), \ldots, \mathrm{y}_m(\vartheta)\}$.

System (33) depends on the strength of singularity s, which is determined as an eigenvalue of the problem. Moreover, the system depends on the conditions of elastic unload-

ing and subsequent plastic reloading, that is, on $\text{sign}(\mathbf{Q}\cdot\dot{\boldsymbol{\sigma}})$ and $f(\boldsymbol{\sigma},\sigma_m)$. Consistently with the assumption of small deformations, a straight path motion of particles is assumed (Fig. 4). Thus, a generic particle ahead of the crack-tip experiences *elastic unloading* at $\vartheta = \vartheta_1$, when:

$$\mathbf{Q}\cdot\dot{\boldsymbol{\sigma}} \leq 0. \tag{34}$$

In the elastic unloading sector, the plastic multiplier vanishes, and the constitutive rate relationships (21) reduce to the linear isotropic elastic relations. Throughout this sector, the value of equivalent stress in the matrix material σ_m remains constant for each material particle and equal to the value assumed at the elastic unloading angle ϑ_1:

$$\sigma_m(\mathrm{r},\vartheta) = \sigma_m(\mathrm{r}_1,\vartheta_1), \qquad \text{for } \vartheta_1 \leq \vartheta \leq \vartheta_2, \tag{35}$$

where ϑ_2 indicates the plastic reloading angle and r_1 singles out the material particle under consideration (Fig. 4). The representation (24) of σ_m and condition (35) imply:

$$\mathrm{y}_m(\vartheta) = (\mathrm{r}_1/\mathrm{r})^s \mathrm{y}_m(\vartheta_1), \quad \text{for } \vartheta_1 \leq \vartheta \leq \vartheta_2. \tag{36}$$

The straight trajectory of a generic particle is defined through the geometric relation:

$$\mathrm{r}\sin\vartheta = \mathrm{r}_1 \sin\vartheta_1. \tag{37}$$

The value of σ_m must remain constant in the elastic sector and thus, in this sector, function $\mathrm{y}_m(\vartheta)$ must have the following dependence on the polar coordinate ϑ:

$$\mathrm{y}_m(\vartheta) = (\sin\vartheta_1/\sin\vartheta)^{-s} \mathrm{y}_m(\vartheta_1), \quad \text{for } \vartheta_1 \leq \vartheta \leq \vartheta_2. \tag{38}$$

Plastic reloading on crack flanks occurs when the particle reaches a stress state which lies on the yield surface left at unloading. Thus, reloading takes place at the angle ϑ_2, when:

$$f(\boldsymbol{\sigma}(\mathrm{r}_2,\vartheta_2),\sigma_m(\mathrm{r}_1,\vartheta_1)) = 0. \tag{39}$$

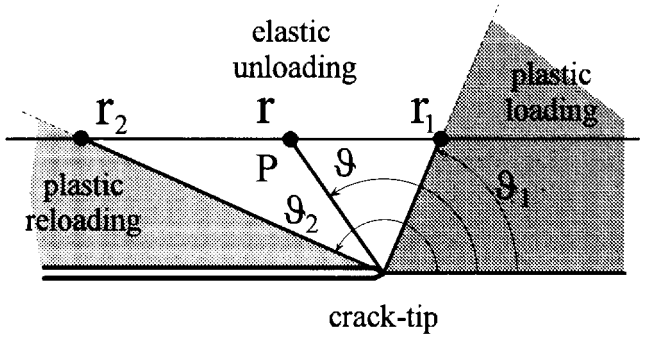

Fig. 4. Loading history of a generic material particle near to the crack-tip.

By using relation (38), the reloading condition (39) becomes:

$$2\Phi \cosh\left[\frac{q_2}{2}\,\frac{y_4(\vartheta_2)+y_5(\vartheta_2)+y_6(\vartheta_2)}{y_m(\vartheta_1)}\left(\frac{\sin\vartheta_2}{\sin\vartheta_1}\right)^{-s}\right]+\frac{3\underline{J}_2(\vartheta_2)}{y_m^2(\vartheta_1)}\left(\frac{\sin\vartheta_2}{\sin\vartheta_1}\right)^{-2s}=1+\Phi^2, \tag{40}$$

where $\underline{J}_2(\vartheta)$ corresponds to:

$$\underline{J}_2=\tfrac{1}{3}(y_4^2+y_5^2+y_6^2-y_4y_5-y_4y_6-y_5y_6)+y_3^2. \tag{41}$$

If representations (23) and (24) are substituted into eqn (10), the following expression for the dimensionless plastic modulus $h = H/E$ is obtained:

$$h=\frac{3h_m}{(1-\phi)y_m^2}(Q_{rr}y_4+Q_{\vartheta\vartheta}y_5+Q_{33}y_6+2Q_{r\vartheta}y_3)^2, \tag{42}$$

where $h_m = H_m/E$.

Mode I and Mode II symmetry conditions restrict the study to the interval $0 \le \vartheta \le \pi$ and yield appropriate boundary conditions ahead crack-tip.

In particular, Mode I loading condition implies at $\vartheta = 0$:

$$v_\vartheta(r,0)=\sigma_{r\vartheta}(r,0)=0, \tag{43}$$

and regularity of the stress and velocity functions ahead of the crack-tip implies:

$$v_{r,\vartheta}(r,0)=\sigma_{rr,\vartheta}(r,0)=\sigma_{\vartheta\vartheta,\vartheta}(r,0)=\sigma_{33,\vartheta}(r,0)=0. \tag{44}$$

Thus, the following boundary conditions have to be prescribed, in terms of functions y_i:

$$y_2(0)=y_3(0)=y_1'(0)=y_4'(0)=y_5'(0)=y_6'(0)=0. \tag{45}$$

Moreover, Mode II loading condition implies at $\vartheta = 0$:

$$v_r(r,0)=\sigma_{rr}(r,0)=\sigma_{\vartheta\vartheta}(r,0)=\sigma_{33}(r,0)=0, \tag{46}$$

and regularity of the stress and velocity functions ahead of the crack-tip implies:

$$v_{\vartheta,\vartheta}(r,0)=\sigma_{r\vartheta,\vartheta}(r,0)=\sigma_{33,\vartheta}(r,0)=0. \tag{47}$$

Thus, the following boundary conditions have to be prescribed, in terms of functions y_i:

$$y_1(0)=y_4(0)=y_5(0)=y_6(0)=y_2'(0)=y_3'(0)=0. \tag{48}$$

Two more boundary conditions, which hold both for Mode I and Mode II, are obtained from the condition that the crack surfaces are traction free, that is, stress components $\sigma_{\vartheta\vartheta}$ and $\sigma_{r\vartheta}$ must vanish at $\vartheta = \pi$:

$$y_3(\pi) = y_5(\pi) = 0. \tag{49}$$

Finally, continuity of functions $y_i(\vartheta)$ has to be imposed at elastic–plastic boundaries. In fact, DRUGAN and RICE [1984] proved that all stress components must be continuous for quasi-static problems in elastoplastic materials with positive isotropic hardening and associative flow-rule.

It is important to remark that all equations reported in this section hold true both in plane strain and in plane stress. The plane stress case corresponds to the condition $y_6 = 0$. In the next sections, the plane stress and plane strain cases are considered in separate ways for Mode I and Mode II, respectively. Moreover, it should be noted that the equations derived in the next sections are referred to plastic sectors, in fact, for the elastic sectors the governing system of equation are well known and can be obtained under the condition $\Lambda = 0$.

IV. MODE I: PLANE STRAIN

The plane strain condition:

$$v_3 = \dot{\varepsilon}_{33} = 0, \tag{51}$$

together with the compatibility relations (19) have to be introduced into the constitutive relations (21) to obtain, with the equilibrium eqns (20), a system of seven first order PDEs in the unknown functions σ_{rr}, $\sigma_{\vartheta\vartheta}$, $\sigma_{r\vartheta}$, σ_{33}, v_r, v_ϑ, and σ_m. In particular, constitutive equations $(21_{1,3})$, expression (9) for the plastic multiplier, and plane strain condition (51) yield the following system of equations:

$$\begin{aligned}(h + Q_{rr}^2)\Sigma_{rr} - (\nu h - Q_{rr}Q_{33})\Sigma_{33} &= y_1 h + (\nu h - Q_{rr}Q_{\vartheta\vartheta})\Sigma_{\vartheta\vartheta} - 2Q_{rr}Q_{r\vartheta}\Sigma_{r\vartheta},\\ -(\nu h - Q_{rr}Q_{33})\Sigma_{rr} + (h + Q_{33}^2)\Sigma_{33} &= (\nu h - Q_{33}Q_{\vartheta\vartheta})\Sigma_{\vartheta\vartheta} - 2Q_{33}Q_{r\vartheta}\Sigma_{r\vartheta}.\end{aligned} \tag{52}$$

Eqns $(29_{1,3})$ make explicit that $\Sigma_{\vartheta\vartheta}$ and $\Sigma_{r\vartheta}$ do not depend on the components of $\mathbf{y}'$. Therefore, functions Σ_{rr} and Σ_{33} follow from eqns (52) in a form that is independent of $\mathbf{y}'$. In particular, Σ_{rr} can be expressed as:

$$\begin{aligned}\Sigma_{rr} = \frac{1}{\Delta}\{&\Sigma_{\vartheta\vartheta}[\nu(1+\nu)h + \nu Q_{33}(Q_{33} - Q_{\vartheta\vartheta}) - Q_{rr}(\nu Q_{33} + Q_{\vartheta\vartheta})]\\ &+ -2\Sigma_{r\vartheta}Q_{r\vartheta}(\nu Q_{33} + Q_{rr}) + y_1(h + Q_{33}^2)\},\end{aligned} \tag{53}$$

where:

$$\Delta = (1 - \nu^2)h + Q_{33}^2 + Q_{rr}^2 + 2\nu Q_{rr}Q_{33}, \tag{54}$$

is always different from zero. Having Σ_{rr}, a substitution in (52_2) gives the expression for Σ_{33}:

$$\Sigma_{33} = \frac{1}{h + Q_{33}^2} [\nu h(\Sigma_{rr} + \Sigma_{\vartheta\vartheta}) - Q_{33}(\Sigma_{rr}Q_{rr} + \Sigma_{\vartheta\vartheta}Q_{\vartheta\vartheta} + 2\Sigma_{r\vartheta}Q_{r\vartheta})]. \tag{55}$$

A substitution of Σ_{rr} and Σ_{33} into eqns $(29_{2,4})$ yields the explicit expressions for y_4' and y_6':

$$y_4' = s y_4 \cot\vartheta + 2y_3 + (\Sigma_{rr}/\sin\vartheta), \tag{56}$$

$$y_6' = s y_6 \cot\vartheta + (\Sigma_{33}/\sin\vartheta). \tag{57}$$

By using eqns (53), (55) and $(29_{1,3})$ for Σ_{rr}, Σ_{33}, $\Sigma_{r\vartheta}$, and $\Sigma_{\vartheta\vartheta}$, the expressions for y_1' and y_2' can be obtained from $(19_{2,3})$ and (21):

$$y_1' = (1 - s)y_2 + 2s[(1 + \nu)\Sigma_{r\vartheta} + \underline{\Lambda} Q_{r\vartheta}], \tag{58}$$

$$y_2' = -y_1 + s[\Sigma_{\vartheta\vartheta} - \nu(\Sigma_{rr} + \Sigma_{33}) + \underline{\Lambda} Q_{\vartheta\vartheta}], \tag{59}$$

where $\underline{\Lambda} = \mathbf{Q}\cdot\boldsymbol{\Sigma}/h$ be written as:

$$\underline{\Lambda} = \frac{1}{h}(Q_{rr}\Sigma_{rr} + Q_{\vartheta\vartheta}\Sigma_{\vartheta\vartheta} + Q_{33}\Sigma_{33} + 2Q_{r\vartheta}\Sigma_{r\vartheta}). \tag{60}$$

Finally, eqn (30) yields:

$$y_m' = s y_m \cot\vartheta + \Sigma_m/\sin\vartheta, \tag{61}$$

where Σ_m, defined by (30) by using (8), can be cast in the following form:

$$\Sigma_m = \underline{\Lambda}\,\frac{3h_m}{(1 - \phi)y_m}\left[\alpha(y_4 + y_5 + y_6) + \frac{3J_2}{y_m}\right]. \tag{62}$$

Eqs. (25), (26), (56–59), and (61) form the first order ODEs system, which governs the near-tip stress and velocity fields.

IV.1. *Boundary conditions*

The Mode I symmetry conditions (43) and (44) imply the vanishing of the values of the nonsymmetric components of stress and velocity functions at $\vartheta = 0$. It should be noted that only four of the boundary conditions (45) are independent. Moreover, the boundary conditions (49) at $\vartheta = \pi$ are of homogeneous type. Therefore, the normalization condition $y_5(0) = 1$, is employed to avoid the trivial solution.

To solve the system (33) of ODEs the Runge–Kutta procedure is used. This approach requires the knowledge of initial values of the functions y_i. The value for $y_4(0)$ is not specified by the boundary conditions (48), and it is not possible to obtain it from the governing system of eqn (56–59), evaluated at $\vartheta = 0$. Therefore, the position $y_4(0) = p$ is made and the values of s and p are initially guessed.

In addition to the boundary conditions (45) and (46), the following conditions on $y_6(0)$ and $y_m(0)$ can be imposed:

$$y_6(0) - \nu(1+p) - \frac{\underline{\Lambda}(0)}{s}\left[\alpha(0) + \frac{2y_6(0) - 1 - p}{2y_m(0)}\right] = 0, \tag{63}$$

$$\frac{3\underline{J}_2(0)}{y_m^2(0)} + 2\Phi\cosh\left[\frac{q_2}{2}\,\frac{1+p+y_6(0)}{y_m(0)}\right] = 1 + \Phi^2, \tag{64}$$

which derive from the plane strain condition (51) and from the yield condition, evaluated at $\vartheta = 0$. The values for $y_6(0)$ and $y_m(0)$ are obtained by solving the nonlinear algebraic system (63-64), using a modified Powell hybrid method. When these values are known, $y_1(0)$ and $y_2'(0)$ result from eqns (53) and (59), evaluated at $\vartheta = 0$:

$$y_1(0) = -s[p - \nu(1 + y_6(0))] + \underline{\Lambda}(0)\left[\alpha(0) + \frac{2p - 1 - y_6(0)}{2y_m(0)}\right], \tag{65}$$

$$y_2'(0) = -y_1(0) - s^2[1 - \nu(p + y_6(0))] + s\underline{\Lambda}(0)\left[\alpha(0) + \frac{2 - p - y_6(0)}{2y_m(0)}\right], \tag{66}$$

where:

$$\alpha(0) = \Phi\,\frac{q_2}{2}\sinh\left(\frac{q_2}{2} + \frac{1+p+y_6(0)}{y_m(0)}\right), \tag{67}$$

$$\underline{\Lambda}(0) = -\frac{s(1-\phi)y_m^2}{3h_m}\left[(1+p+y_6(0))\alpha(0) + \frac{3\underline{J}_2(0)}{y_m(0)}\right]^{-1}, \tag{68}$$

$$\underline{J}_2(0) = \tfrac{1}{3}\left(1 + p^2 + y_6^2(0) - p - y_6(0) - py_6(0)\right). \tag{69}$$

Eqns (45), (63-66) give all values of $\mathbf{y}(0)$ and $\mathbf{y}'(0)$. It is worth noting that the knowledge of the values of $\mathbf{y}'(0)$ is important in the present problem. In fact, the value of y_4' at $\vartheta = 0$ cannot be derived from eqn (56), and thus the numerical procedure cannot start. The knowledge of $\mathbf{y}'(0)$ makes a Taylor series expansion of functions y_i possible, in the form:

$$\mathbf{y}(\varepsilon) = \mathbf{y}(0) + \varepsilon\mathbf{y}'(0) + o(\varepsilon). \tag{70}$$

Therefore, the numerical solution can be obtained starting at $\vartheta = \varepsilon$, rather than at $\vartheta = 0$. The integration can finally be performed, with the assigned values of p and s. On the basis of a check on the values $y_3(\pi)$ and $y_5(\pi)$, the guessed values of p and s are reassigned, and the process is iterated using a modified Powell hybrid method, until $y_3(\pi)$ and $y_5(\pi)$ are found to be sufficiently close to zero. Finally, all the results are normalised through the condition:

$$y_m(\vartheta_1) = 1. \tag{71}$$

IV.2. *Results*

In Table 1 the computed values of the singularity s, the elastic unloading angle ϑ_1 and the reloading angle ϑ_2 are reported for different values of the porosity parameter

Table 1. Values of the singularity exponent s and angles ϑ_1 and ϑ_2, for $\nu = 1/3$, corresponding to $\alpha_G = 0.001$ and 0.1, for different values of porosity Φ, in Mode I plane strain conditions

	α_G					
	0.001			0.1		
Φ	s	ϑ_1	ϑ_2	s	ϑ_1	ϑ_2
0.000	−0.05640	136.965	138.444	−0.20956	122.012	175.318
0.001	−0.04595	135.908	138.343	−0.23659	116.635	178.990
0.005	−0.03697	134.446	139.978	−0.25221	110.897	179.996
0.010	−0.03224	132.885	142.724	−0.25912	107.024	180.000
0.020	−0.02750	127.912	151.357	−0.26409	102.195	180.000
0.030	−0.02635	117.106	165.224	−0.26521	98.974	180.000
0.040	−0.02694	105.258	175.009	−0.26486	96.543	180.000
0.050	−0.02746	97.471	178.510	−0.26382	94.585	180.000
0.100	−0.02810	79.209	180.000	−0.25527	88.127	180.000
0.150	−0.02764	70.696	180.000	−0.24561	84.048	180.000

Φ, for $q_2 = 1$. A low hardening case ($\alpha_G = 0.001$) and a high hardening case ($\alpha_G = 0.1$) are analyzed. In the case $\Phi = 0$, the results of the *J_2-flow theory* are fully recovered (see PONTE CASTAÑEDA [1987], in which, however, a different definition of α_G is used). All reported results refer, for conciseness, to $\nu = \frac{1}{3}$. From Table 1 it can be concluded that the absolute value of the singularity exponent, as well as the unloading angle and the size of the reloading sector strongly decrease in highly porous metals, for small strain hardening. The first of these effects suggest the conclusion that porosity should have a stabilizing effect on crack growth. However, for high strain hardening ($\alpha_G = 0.1$), the singularity exponent s reaches a minimum for a porosity Φ around the value 0.03.

The angular distribution of the stress and velocity functions y_i, normalized under condition (71), are shown in Figs. 5, 6, 7, and 8 for different values of the porosity, for $\alpha_G = 0.001$ and 0.1. From the figures it can be noted that for low values of porosity the stress component σ_{33}, orthogonal to the deformation plane, is intermediate between the radial and circumpherential stresses σ_{rr} and $\sigma_{\vartheta\vartheta}$. For high values of porosity, the stress components σ_{rr} and $\sigma_{\vartheta\vartheta}$ coincide in the whole plastic sector ahead of the crack-tip. Therefore, differently from the Drucker–Prager model, the stress state ahead of the crack-tip does not tend to the hydrostatic stress state. Moreover, it is important to emphasize that, coherently with the results of DRUGAN and RICE [1984], continuous stress fields have been found. However, the obtained stress fields share a similarity to the asymptotic fields obtained by DRUGAN and MIAO [1992] in the perfectly plastic limit of the Gurson model. In fact, in correspondence of the critical value of porosity at which Drugan and Maio find jumps in the angular distribution of stress, the obtained fields show a definite change in shape, but still remain continuous.

V. MODE I: PLANE STRESS

The plane stress condition:

$$\sigma_{33} = \dot{\sigma}_{33} = y_6 = 0, \tag{72}$$

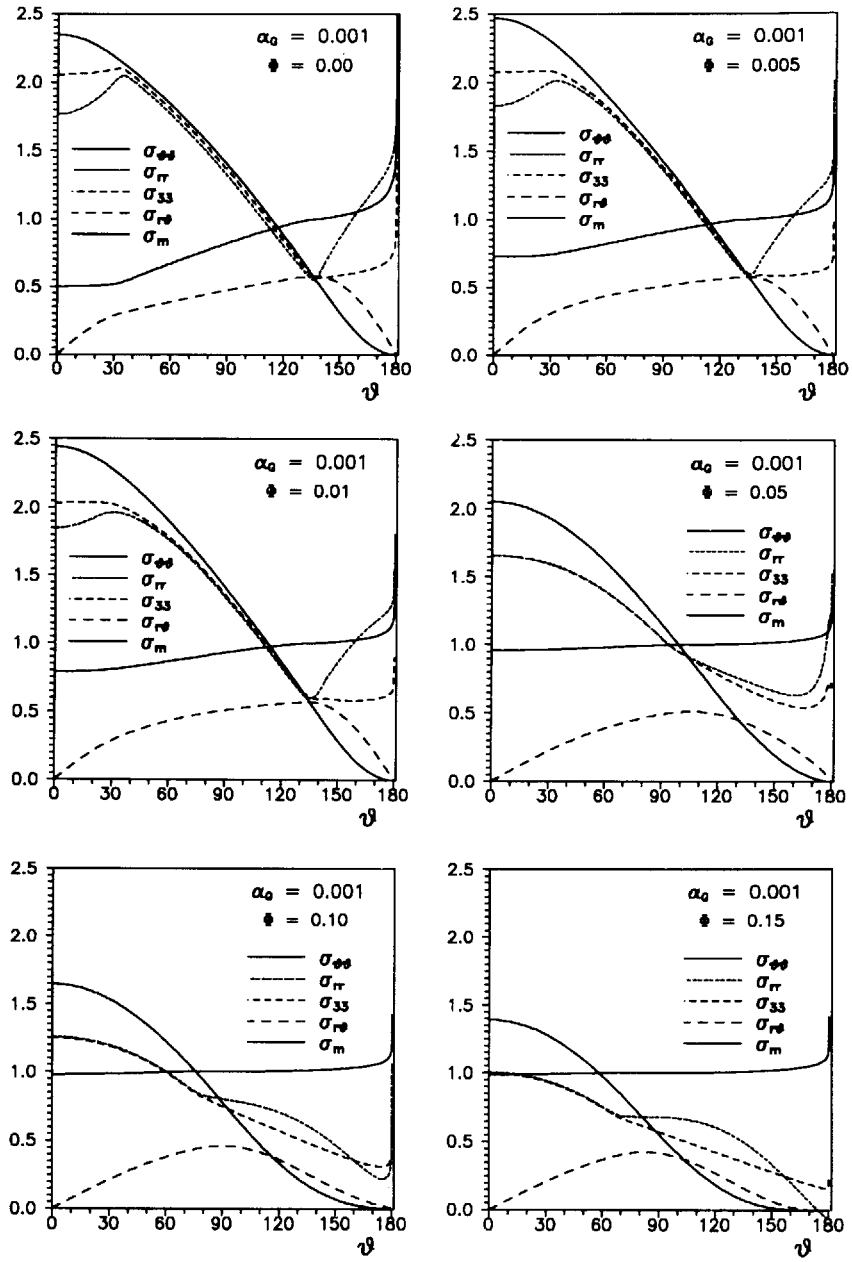

Fig. 5. Angular distribution of stress functions near crack-tip for small hardening of the matrix material ($\alpha_G = 0.001$), corresponding to different values of the porosity parameter Φ, in Mode I, plane strain conditions. The case $\phi = 0$ corresponds to the *J_2-flow theory*.

together with the compatibility relations (19) may be substituted into the constitutive relation (21_1) to obtain:

$$\Sigma_{rr} = \frac{1}{h + Q_{rr}^2}\left[y_1 h + \Sigma_{\vartheta\vartheta}(\nu h - Q_{rr}Q_{\vartheta\vartheta}) - 2\Sigma_{r\vartheta}Q_{rr}Q_{r\vartheta}\right], \tag{73}$$

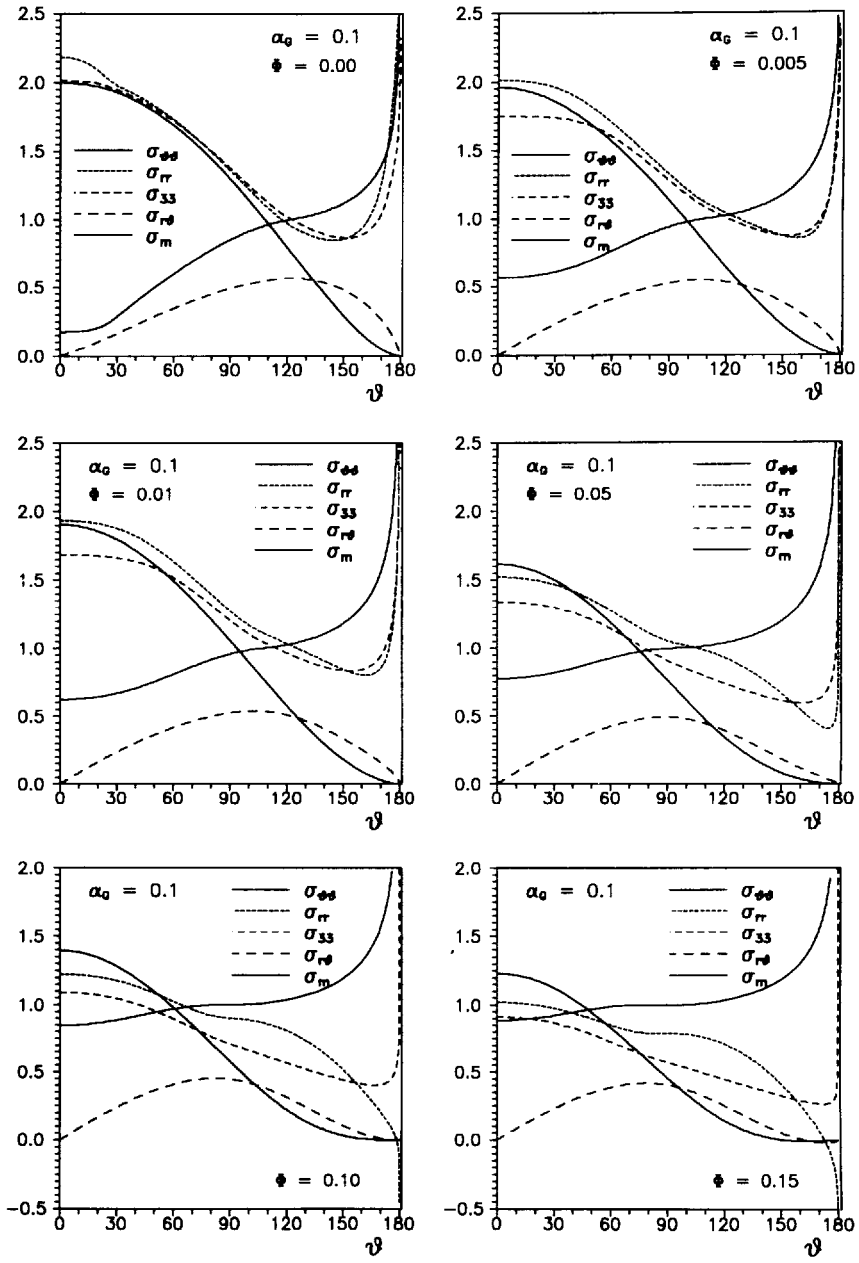

Fig. 6. Angular distribution of stress functions near crack-tip for high hardening of the matrix material ($\alpha_G = 0.1$), corresponding to different values of the porosity parameter Φ, in Mode I, plane strain conditions. The case $\phi = 0$ corresponds to the *J_2-flow theory*.

where the dimensionless stress rates (28) have been employed. From ($29_{1,3}$), (31) and (42), it can be concluded that Σ_{rr} depends on functions y_i, but it is independent of their derivatives. Thus, y_4' results from (29_2) to be:

$$y_4' = s y_4 \cot\vartheta + 2y_3 + \Sigma_{rr}/\sin\vartheta, \tag{74}$$

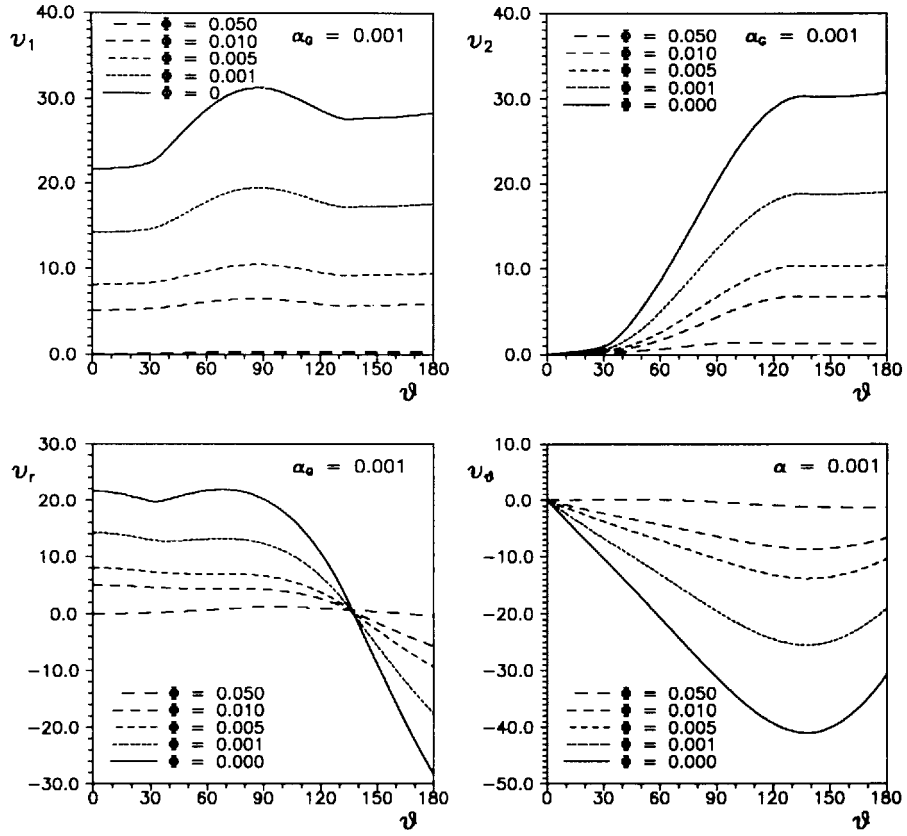

Fig. 7. Comparison between the velocity functions near crack-tip for small hardening of the matrix material ($\alpha_G = 0.001$), corresponding to different values of the porosity parameter Φ, in Mode I, plane strain conditions.

where Σ_{rr} is given by (73). Explicit expressions for y_1' and y_2' can be directly obtained from ($27_{2,3}$) and ($29_{2,3}$) in the form:

$$y_1' = (1 - s)y_2 + 2s[(1 + \nu)\Sigma_{r\vartheta} + \underline{\Lambda}Q_{r\vartheta}], \tag{75}$$

$$y_2' = -y_1 + s(\Sigma_{\vartheta\vartheta} - \nu\Sigma_{rr} + \underline{\Lambda}Q_{\vartheta\vartheta}), \tag{76}$$

where $\underline{\Lambda} = \mathbf{Q}\cdot\boldsymbol{\Sigma}/h$ results to be:

$$\underline{\Lambda} = \frac{1}{h}(Q_{rr}\Sigma_{rr} + Q_{\vartheta\vartheta}\Sigma_{\vartheta\vartheta} + 2Q_{r\vartheta}\Sigma_{r\vartheta}). \tag{77}$$

Moreover, the evolution equation for y_m is readily obtained from (30):

$$y_m' = sy_m \cot\vartheta + \Sigma_m/\sin\vartheta, \tag{78}$$

where Σ_m is defined by using (8), in dimensionless form:

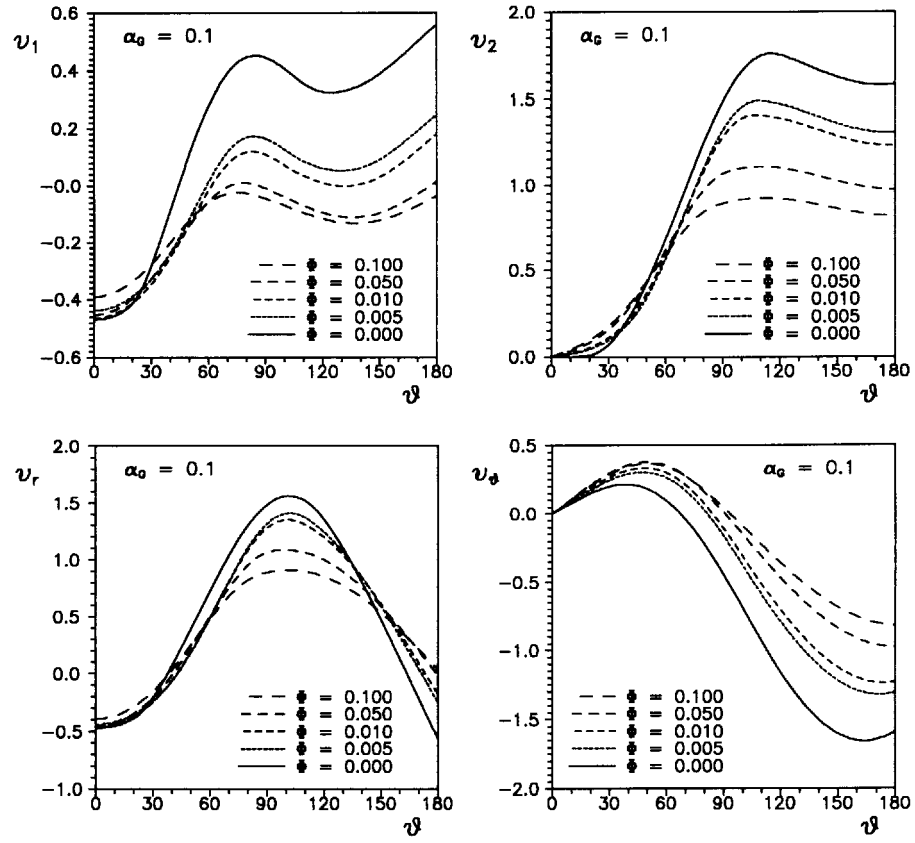

Fig. 8. Comparison between the velocity functions near crack-tip for high hardening of the matrix material ($\alpha = 0.1$), corresponding to different values of the porosity parameter Φ, in Mode I, plane strain conditions.

$$\Sigma_m = \underline{A}\,\frac{3h_m}{(1-\phi)y_m}\left[\alpha(y_4 + y_5) + \frac{3\underline{J}_2}{y_m}\right], \tag{79}$$

and $\underline{J}_2$ results from (41), under the plane stress condition $y_6 = 0$.

Therefore, the system of ODEs defined by (25), (26), (74), (75), (76), and (78), which governs the asymptotic stress and velocity fields near the propagating crack-tip, may be expressed in a form similar to (33).

V.1. *Boundary conditions*

The scheme for solving the system (33) is quite similar to the plane strain case. Now, the normalisation $y_5(0) = 1$ is adopted and the values of $p = y_4(0)$ and s are initially guessed. When eqns (73), (76), and (25) are evaluated at $\vartheta = 0$, the following auxiliary conditions are obtained:

$$y_1(0) = -s\left\{p - \nu - \frac{\underline{A}(0)}{s}\left[\alpha(0) + \frac{2p-1}{2y_m(0)}\right]\right\}, \tag{80}$$

$$y_2'(0) = -y_1(0) - s^2\left\{1 - \nu p - \frac{\underline{A}(0)}{s}\left[\alpha(0) + \frac{2-p}{2y_m(0)}\right]\right\}, \tag{81}$$

$$y_3'(0) = 1 - (1+s)p, \tag{82}$$

where:

$$\underline{A}(0) = -\frac{s(1-\phi)y_m^2}{3h_m}\left[(1+p)\alpha(0) + \frac{3\underline{J}_2(0)}{y_m(0)}\right]^{-1} \tag{83}$$

$$\alpha(0) = \Phi\frac{q_2}{2}\sinh\left(\frac{q_2}{2} + \frac{1+p}{y_m(0)}\right), \qquad \underline{J}_2(0) = \tfrac{1}{3}(1 + p^2 - p). \tag{84}$$

The value of $y_m(0)$ can now be obtained by evaluating the yield condition at $\vartheta = 0$:

$$\frac{3\underline{J}_2(0)}{y_m^2(0)} + 2\Phi\cosh\left[\frac{q_2}{2}\frac{1+p}{y_m(0)}\right] = 1 + \Phi^2. \tag{85}$$

Eqns (45), (80–82) give all values of $\mathbf{y}(0)$ and $\mathbf{y}'(0)$. As in plane strain, all results are finally normalized through (71).

V.2. *Results*

Similarly to the J_2 flow-theory and to the Drucker–Prager model in plane stress, the results in terms of stress components do not depend on the Poisson ratio. Therefore, all results are reported for the case $\nu = \frac{1}{2}$ and $q_2 = 1$. The computed values of the singularity exponent s, the elastic unloading and plastic reloading angles ϑ_1 and ϑ_2 are reported in Table 2 for different values of the porosity. A low hardening ($\alpha_G = 0.001$) and a high hardening ($\alpha_G = 0.1$) cases are considered. When Φ is set equal to zero, the results of the *J_2-flow theory* are fully recovered (see PONTE CASTAÑEDA [1987]).

From Table 2 it can be noted that for high values of porosity the singularity exponent s increases and the size of the plastic sector ahead the crack-tip decreases. Moreover,

Table 2. Values of the singularity exponent s and angles ϑ_1 and ϑ_2, for $\nu = 1/2$, corresponding to $\alpha_G = 0.001$ and 0.1, for different values of porosity Φ, in Mode I plane stress conditions

	α_G					
	0.001			0.1		
Φ	s	ϑ_1	ϑ_2	s	ϑ_1	ϑ_2
0.000	−0.02866	53.202	179.999	−0.23721	73.646	180.000
0.001	−0.02865	53.185	179.999	−0.23710	73.629	180.000
0.005	−0.02858	53.117	179.999	−0.23663	73.561	180.000
0.010	−0.02849	53.034	179.999	−0.23604	73.476	180.000
0.050	−0.02780	52.394	179.998	−0.23131	72.808	180.000
0.100	−0.02693	51.658	179.997	−0.22533	71.995	180.000
0.150	−0.02605	50.980	179.996	−0.21928	71.199	180.000
0.200	−0.02516	50.347	179.995	−0.21310	70.413	180.000

the plastic reloading sector is very thin, as in the cases of the J_2 and Drucker-Prager models. All these effects are less pronounced than in the plane strain case.

The angular distribution of the stress and velocity functions y_i, normalized under the condition (71), are shown in Fig. 9 for different values of the porosity, for $\alpha_G = 0.001$ and $\alpha_G = 0.1$. From the figures it can be concluded that an increase of the parameter

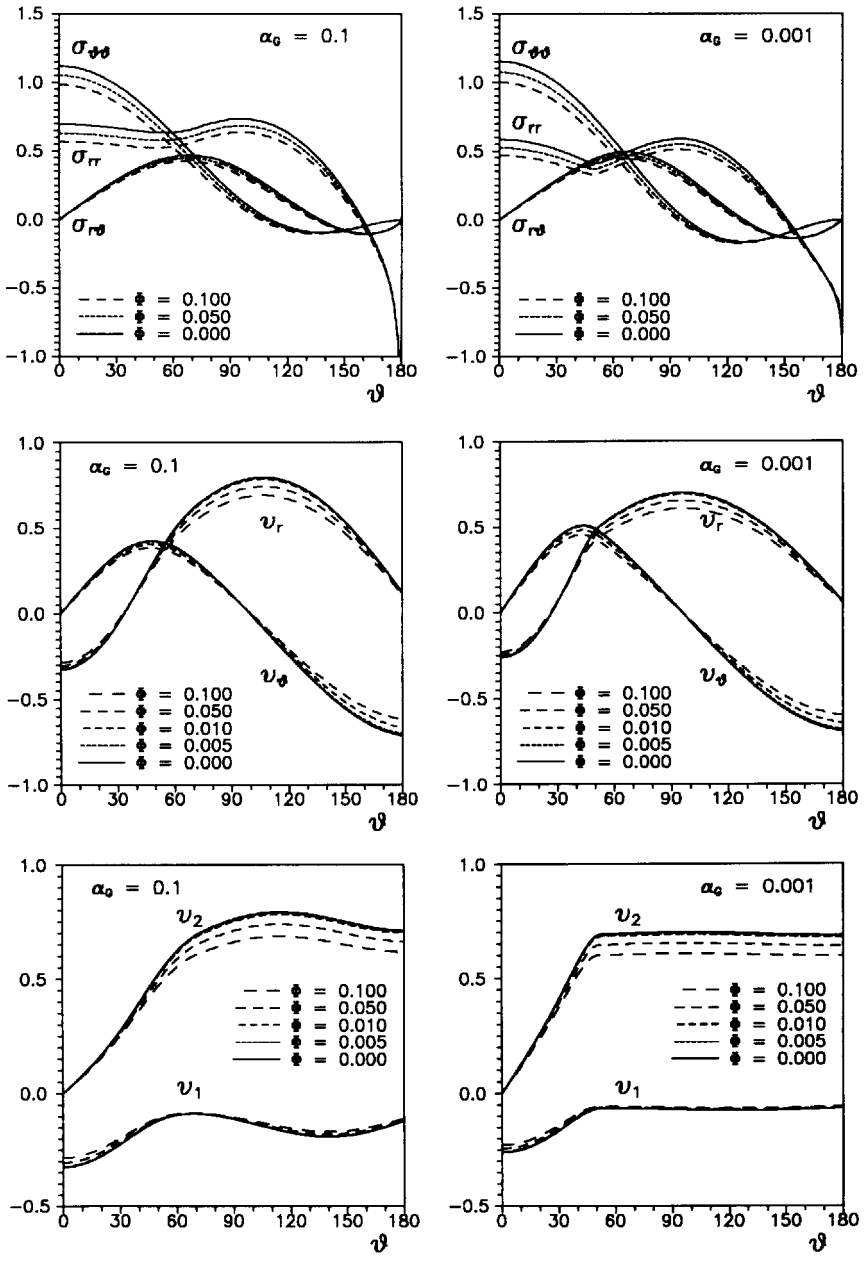

Fig. 9. Stress and velocity angular distributions for small and high hardening of the matrix material (α_G = 0.001, 0.1) corresponding to different values of the porosity parameter Φ, in Mode I, plane stress conditions.

Φ yields a remarkable reduction in the radial stress ahead of the crack-tip, which corresponds to a reduction in the hydrostatic stress state.

VI. MODE II: PLANE STRAIN

Mode II symmetry conditions (48) imply the vanishing of the symmetric components of stress and velocity functions at $\vartheta = 0$. The normalization condition:

$$y_3(0) = 1, \tag{86}$$

is employed to avoid the trivial solution. The boundary conditions (48) do not specify the value of $y_2(0)$, and it is not possible to derive it from the governing system of eqn (56–59) evaluated at $\vartheta = 0$. Therefore, the following position is made:

$$y_2(0) = p, \tag{87}$$

and the values of s and p are initially guessed. The value for $y_m(0)$ results from the yield condition (64) at $\vartheta = 0$, since all values of the stress functions are known in $\vartheta = 0$:

$$y_m(0) = \frac{\sqrt{3}}{1 - \Phi}. \tag{88}$$

The equilibrium eqn (26) evaluated at $\vartheta = 0$, yields:

$$y_5'(0) = -(s + 2). \tag{89}$$

Eqns (48) and (86–87) give $\mathbf{y}(0)$ and some components of $\mathbf{y}'(0)$, but do not specify $y_4'(0)$ and $y_6'(0)$. Moreover, $y_4'(0)$ and $y_6'(0)$ cannot be obtained from eqns (56,57), since these equations assume an indeterminate form at $\vartheta = 0$. Therefore, a Taylor series expansion of functions y_i is performed near $\vartheta = 0$ and $\vartheta = \varepsilon$, namely:

$$\mathbf{y}(\varepsilon) = \mathbf{y}(0) + \varepsilon\mathbf{y}'(0) + o(\varepsilon), \qquad \text{where:} \qquad \mathbf{y}'(0) = \mathbf{y}'(\varepsilon) + o(\varepsilon). \tag{90}$$

Once the values of $\mathbf{y}(0)$ and $\mathbf{y}'(0)$ or $\mathbf{y}'(\varepsilon)$ are known, the numerical procedure can be started from a small value, say ε, of the angular variable ϑ. It should be noted that (90) holds true under the hypothesis of regularity of the functions $\mathbf{y}(\vartheta)$ ahead of the crack-tip. By using eqns (48), (86), and (87) the asymptotic expansion (90) may be written as:

$$\begin{aligned}
y_1(\varepsilon) &= \varepsilon y_1'(\varepsilon) + o(\varepsilon),\\
y_2(\varepsilon) &= p + o(\varepsilon),\\
y_3(\varepsilon) &= 1 + o(\varepsilon),\\
y_4(\varepsilon) &= \varepsilon y_4'(0) + o(\varepsilon),\\
y_5(\varepsilon) &= -\varepsilon(s + 2) + o(\varepsilon),\\
y_6(\varepsilon) &= \varepsilon y_6'(0) + o(\varepsilon).
\end{aligned} \tag{91}$$

Evaluation of the yield condition (1) at $\vartheta = \varepsilon$, and eqns (91) give:

$$y_m(\varepsilon) = \frac{\sqrt{3}}{1 - \Phi} + o(\varepsilon). \tag{92}$$

In view of (91), the dimensionless stress rates (29) assume the following values at $\vartheta = \varepsilon$:

$$\begin{aligned}
\Sigma_{r\vartheta}(\varepsilon) &= -s + o(\varepsilon), \\
\Sigma_{\vartheta\vartheta}(\varepsilon) &= \varepsilon s(s+1) + o(\varepsilon), \\
\Sigma_{rr}(\varepsilon) &= \varepsilon[(1-s)y_4'(0) - 2] + o(\varepsilon), \\
\Sigma_{33}(\varepsilon) &= \varepsilon(1-s)y_6'(0) + o(\varepsilon).
\end{aligned} \tag{93}$$

Moreover, eqns (31) evaluated at $\vartheta = \varepsilon$ become:

$$\begin{aligned}
Q_{r\vartheta}(\varepsilon) &= \frac{3}{2y_m(0)} + o(\varepsilon), \\
Q_{rr}(\varepsilon) &= \alpha(\varepsilon) + \frac{2y_4'(0) - y_6'(0) + s + 2}{2y_m(0)}\varepsilon + o(\varepsilon), \\
Q_{\vartheta\vartheta}(\varepsilon) &= \alpha(\varepsilon) - \frac{2(s+2) + y_4'(0) + y_6'(0)}{2y_m(0)}\varepsilon + o(\varepsilon), \\
Q_{33}(\varepsilon) &= \alpha(\varepsilon) + \frac{2y_6'(0) - y_4'(0) + s + 2}{2y_m(0)}\varepsilon + o(\varepsilon),
\end{aligned} \tag{94}$$

where:

$$\alpha(\varepsilon) = \Phi\left(\frac{q_2}{2}\right)^2 \frac{y_4'(0) + y_6'(0) - (s+2)}{y_m(0)}\varepsilon + o(\varepsilon). \tag{95}$$

Therefore, the dimensionless hardening modulus $h(\varepsilon) = H(\varepsilon)/E$ and $\underline{\Lambda}(\varepsilon)$ can be obtained through substitution of (91–95) into eqns (42) and (60), respectively:

$$h(\varepsilon) = 3h_m \frac{(1-\Phi)^4}{1-\phi} + \sigma(\varepsilon), \tag{96}$$

$$\underline{\Lambda}(\varepsilon) = -\frac{s}{\sqrt{3}h_m} \frac{1-\phi}{(1-\Phi)^3} + \sigma(\varepsilon). \tag{97}$$

Eqn (58) yields the following value of $y_1'(\varepsilon)$:

$$y_1'(\varepsilon) = (1-s)p - 2s^2\left[1 + \nu + \frac{1-\phi}{2h_m(1-\Phi)^2}\right] + o(\varepsilon). \tag{98}$$

A substitution of relations (93) and (94) into eqns (52) gives the following system of two equations, where $y_4'(0)$ and $y_6'(0)$ are unknowns:

$$[1 - s - \gamma_2(2 - \nu + \Phi_2)]y_4'(0) - \gamma_2(2\nu - 1 + \Phi_2)y_6'(0) = 2 + \frac{\nu s(s+1)}{1+\nu} + \frac{y_1'(\varepsilon)}{1-\nu^2} + \gamma_2(s+2)(\nu + 1 - \Phi_2), \tag{99}$$

$$[-\nu(1-s) + \gamma_1(\tfrac{1}{2} - \Phi_1)]y_4'(0) + [1 - s - \gamma_1(1 + \Phi_1)]y_6'(0) = \nu[s(s+1) - 2] + \gamma_1(\tfrac{1}{2} - \Phi_1)(s+2), \tag{100}$$

where the following symbols have been introduced:

$$\gamma_1 = \frac{s(1-\phi)}{3h_m(1-\Phi)^2}, \qquad \gamma_2 = \frac{\gamma_1}{2(1-\nu^2)}, \qquad \Phi_1 = \Phi\left(\frac{q_2}{2}\right)^2, \qquad \Phi_2 = 2\Phi_1(1+\nu). \tag{101}$$

Now, values of $y_4'(0)$ and $y_6'(0)$ can be obtained by solving eqns (99–100). When $y_1'(\varepsilon)$, $y_4'(0)$, and $y_6'(0)$ are substituted into eqns (91), the values of all the stress and velocity functions at $\vartheta = \varepsilon$ are known. Then, the numerical integration may be performed, starting at $\vartheta = \varepsilon$. At the extreme $\vartheta = \pi$ a check is made on y_3 and y_5. On the basis of this check, the values of p and s are reassigned and the process is iterated, adopting the usual scheme.

VI.1. *Results*

In Tables 3 and 4 the computed values of the singularity exponent s, the elastic unloading angles ϑ_1, ϑ_3, and the reloading angles ϑ_2 and ϑ_4 are reported for different values of the porosity parameter Φ. In these tables, the following hardening values are considered: $\alpha_G = 0.001$, 0.01, and 0.75. All reported results refer, for conciseness, to $\nu = \frac{1}{3}$ and $q_2 = 1$. The case $\Phi = 0$ corresponds to a material without porosity, therefore, the

Table 3. Values of the singularity exponent s and angles ϑ_1 and ϑ_2, for $\nu = 1/3$, corresponding to $\alpha_G = 0.001$ and 0.1, for different values of porosity Φ, in Mode II plane strain conditions

	α_G					
	0.001			0.1		
Φ	s	ϑ_1	ϑ_2	s	ϑ_1	ϑ_2
0.000	−0.029120	20.950	179.911	−0.238744	34.542	180.000
0.010	−0.028899	21.048	179.909	−0.237572	34.624	180.000
0.050	−0.028029	21.432	179.901	−0.232826	34.950	180.000
0.100	−0.026967	21.894	179.889	−0.226761	35.356	180.000
0.150	−0.025926	22.339	179.877	−0.220536	35.760	180.000
0.200	−0.024900	22.769	179.864	−0.214134	36.162	180.000

Table 4. Values of s, ϑ_1, ϑ_2, ϑ_3, and ϑ_4, for $\nu = 1/3$ and $\alpha_G = 0.75$, corresponding to different values of porosity Φ, in Mode II plane strain conditions

Φ	s	ϑ_1	ϑ_2	ϑ_3	ϑ_4
0.000	−0.467330	41.519	129.343	137.010	180.000
0.050	−0.464618	41.854	125.024	136.440	180.000
0.100	−0.461673	42.198	121.555	135.892	180.000
0.150	−0.458461	42.551	118.497	135.360	180.000
0.200	−0.454941	42.914	115.684	134.840	180.000

results of the *J_2-flow theory* are fully recovered (see PONTE CASTAÑEDA [1987]). The angular distribution of the stress and velocity functions y_i, normalized under the condition:

$$y_m(\vartheta_1) = 1, \tag{102}$$

are shown in Figs. 10 and 11, for different values of the porosity parameter Φ. The value of the mean stress and the equivalent stress in the matrix material are reported in Fig. 12.

As in the case of the *J_2-flow theory*, two elastic sectors appear in the solution. Moreover, for high strain hardening, the solution tends to the linear elastic solution. From the tables and figures it can be noted that the absolute value of the singularity, as well as the size of the elastic sectors decrease, for high values of porosity. Moreover, an increase in the porosity yields a flatten in the graphs of all stress and velocity functions. From Fig. 10 it can be noted that a lowering in the hardening yields a coincidence of the radial and the out-of-plane components of stress. This circumstance, which occurs also for the J_2-flow theory, is in agreement with the perfectly plastic limit, where a centred fan sector appears ahead of the crack tip. Finally, it is important to mention that (see Fig. 12) the mean normal stress and parameter σ_m are very little influenced by the porosity, for small strain hardening. This circumstance is in contrast with the results obtained in the case of Mode I condition. In addition, it is important to mention that the mean normal stress and parameter σ_m have, at small strain hardening, a weak dependence on the angular coordinate ϑ. This fact is coherent with the perfectly plastic limit, where σ_m is constant. Finally, it should be noted that the mean normal stress remains small for Mode II loading condition.

VII. MODE II: PLANE STRESS

The boundary conditions (48), (86–88), at $\vartheta = 0$, and (49), at $\vartheta = \pi$, are still valid for plane stress, Mode II loading. In this case $y_4'(0)$ is undetermined. A Taylor series expansion of function $\mathbf{y}(\vartheta)$ yields eqns (93–95) for the components of $\boldsymbol{\Sigma}$ and $\mathbf{Q}$, where now $y_6'(0) = y_6(0) = 0$. A substitution of these relations into eqns (73) evaluated at $\vartheta = 0$ gives:

$$\Sigma_{rr}(\varepsilon) = \varepsilon\left\{y_1'(\varepsilon) + \nu s(s+1) + \gamma_1\left[\Phi_1(y_4'(0) - s - 2) + y_4'(0) + 1 + \frac{s}{2}\right]\right\} + o(\varepsilon). \tag{103}$$

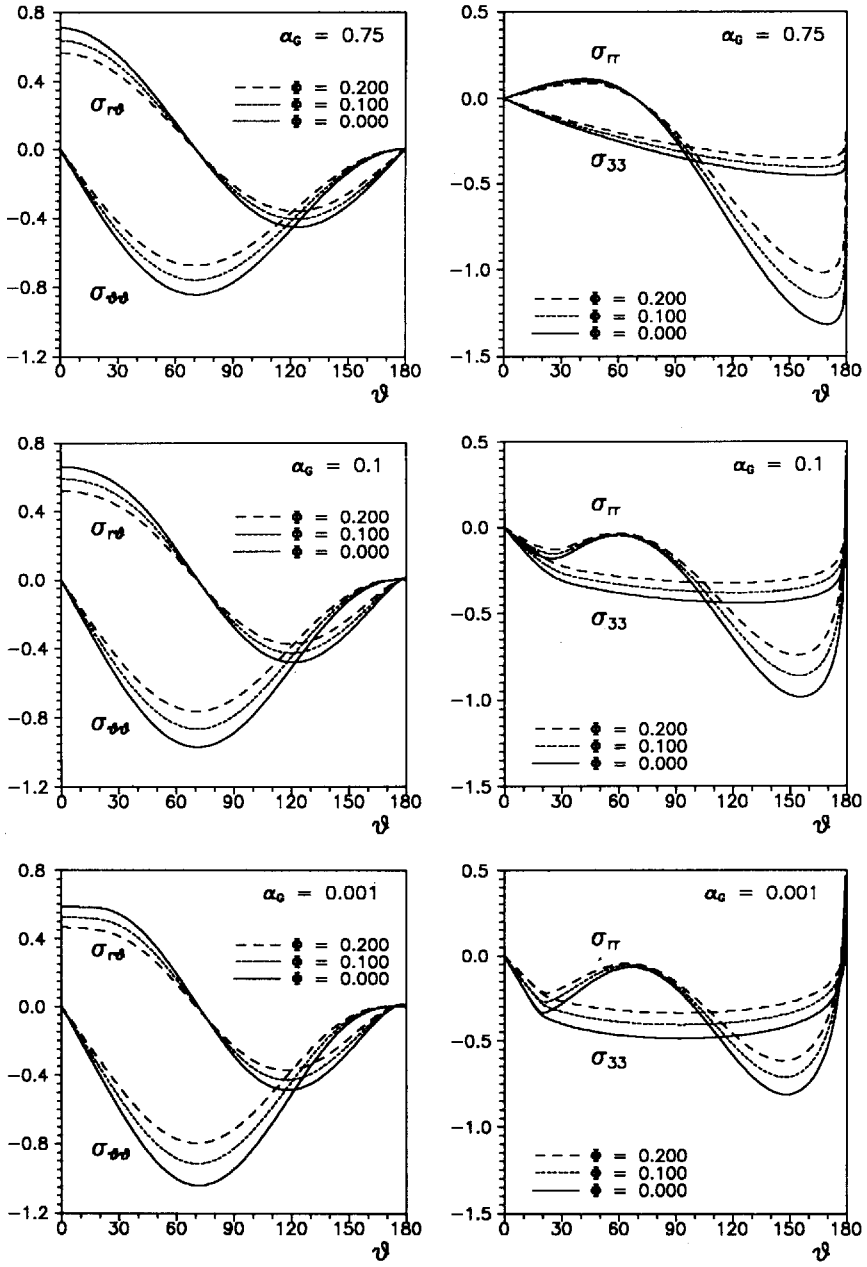

Fig. 10. Angular distribution of stress functions near crack-tip for various values of hardening of the matrix material ($\alpha_G = 0.001, 0.1, 0.75$), corresponding to different values of the porosity parameter Φ, in Mode II, plane strain conditions. The case $\phi = 0$ corresponds to the *J_2-flow theory*.

Finally, by equating eqns (93) and (103) and by employing relation (98) for $y_1'(\varepsilon)$, which holds true in plane stress condition also, the following value for $y_4'(0)$ is derived:

$$y_4'(0) = \frac{1}{D}\left\{2 + (1-s)p - s^2(2+\nu) + s\nu + \gamma_1\left[1 - \frac{5}{2}s - \Phi_1(s+2)\right]\right\}, \qquad (104)$$

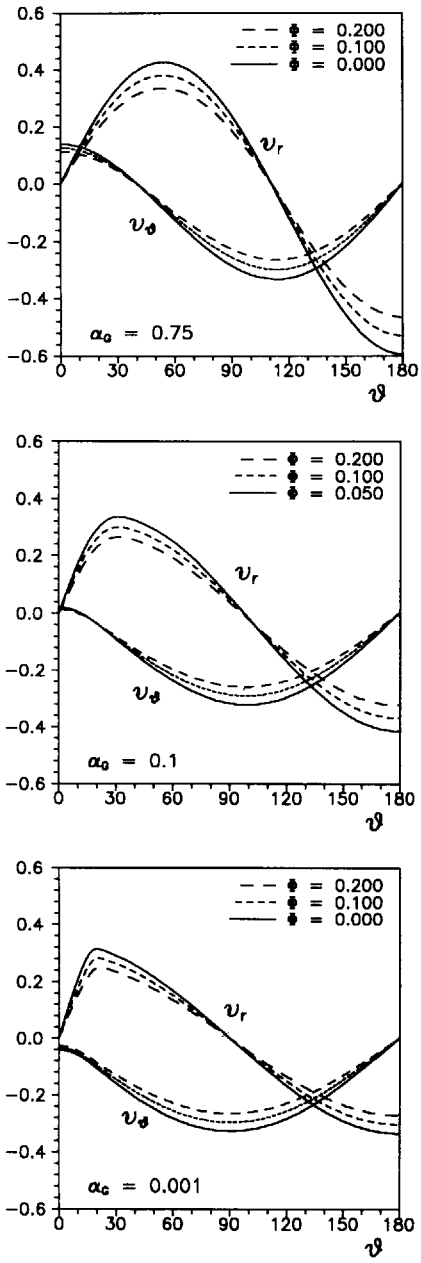

Fig. 11. Angular distribution of velocity functions near crack-tip for various values of hardening of the matrix material (α_{Gi} = 0.1, 0.1, 0.75), corresponding to different values of the porosity parameter Φ, in Mode II, plane strain conditions. The case $\phi = 0$ corresponds to the *J_2-flow theory*.

where:

$$D = 1 - s - \gamma_1[1 + \Phi_1]. \tag{105}$$

When the values of $y_1'(\varepsilon)$ and $y_4'(0)$ are known, all the values of stress and velocity functions at $\vartheta = \varepsilon$ are derived through eqns (91). Thus, the integration may be performed

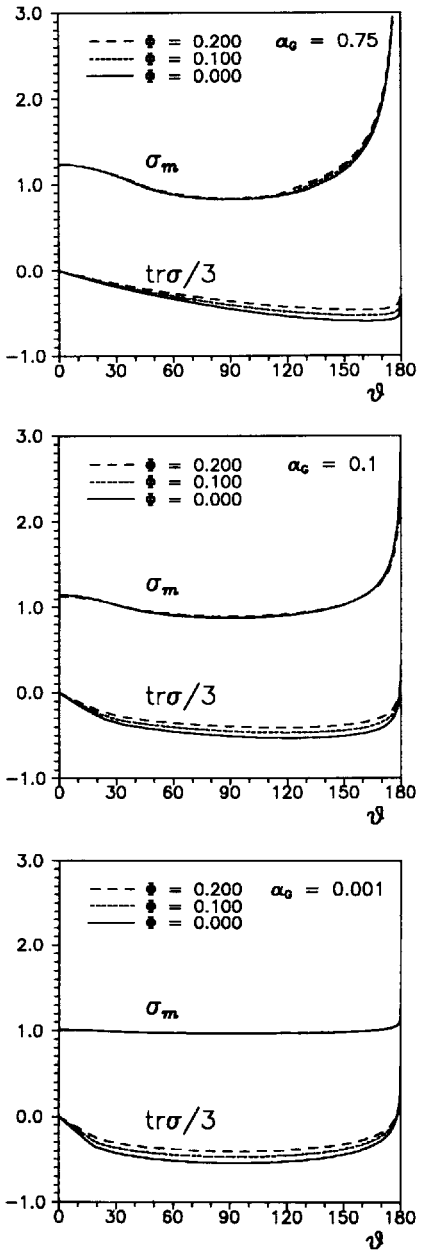

Fig. 12. Angular distribution of mean stress and equivalent stress in the matrix material, for various values of hardening (α_G = 0.001, 0.1, 0.75), corresponding to different values of the porosity parameter Φ, in Mode II, plane strain conditions.

starting at $\vartheta = \varepsilon$ and the procedure is iterated, with a check on the values of $y_3(\pi)$ and $y_3(\pi)$.

VII.1. *Results*

In Tables 5 and 6 the computed values of the singularity s, the elastic unloading angles ϑ_1, ϑ_3 and the reloading angles ϑ_2, ϑ_4 are reported for different values of the porosity

Table 5. Values of the singularity exponent s and angles ϑ_1 and ϑ_2, ϑ_3, and ϑ_4, for $\nu = 1/2$, corresponding to $\alpha_G = 0.001$ and 0.1, for different values of porosity Φ, in Mode II plane stress conditions

	α_G							
	0.001			0.1				
Φ	s	ϑ_1	ϑ_2	s	ϑ_1	ϑ_2	ϑ_3	ϑ_4
0.000	−0.02631	26.124	179.791	−0.21907	40.269	106.554	123.498	180.000
0.010	−0.02616	26.166	179.788	−0.21800	40.305	106.280	123.384	180.000
0.050	−0.02555	26.334	179.779	−0.21367	40.448	105.200	122.925	180.000
0.100	−0.02477	26.541	179.768	−0.20814	40.623	103.885	122.347	180.000
0.150	−0.02398	26.746	179.756	−0.20249	40.792	102.606	121.763	180.000
0.200	−0.02318	26.948	179.744	−0.19670	40.955	101.362	121.170	179.999

parameter Φ. In these tables, the following hardening values are considered: $\alpha_G = 0.001$, 0.1, and 0.75. All reported results refer, for conciseness, to $\nu = \frac{1}{2}$ and to $q_2 = 1$. When $\Phi = 0$, the results of the *J_2-flow theory* are fully recovered (see PONTE CASTAÑEDA [1987]). The angular distribution of the stress and velocity functions y_i, normalized under the condition $y_m(\vartheta_1) = 1$, are shown in Fig. 13, for different values of the porosity parameter Φ. The value of the mean stress and of the effective stress in the matrix material σ_m are reported in Fig. 14.

It should be noted that results are very similar to the plane strain case. This circumstance is in full agreement with the results of the *J_2-flow theory*. The observations drawn in the case of plane strain are still pertinent. The main difference with respect to the Mode II plane strain case is the more frequent appearance of two elastic unloading sectors.

VIII. CONCLUSIONS

In this article, the near tip fields of a steadily propagating crack under Mode I and Mode II loading conditions have been obtained for the Gurson incremental elastoplastic model with constant porosity, by adopting the solution procedure proposed by PONTE CASTAÑEDA [1987].

The obtained results fit coherently with the previous analysis for the perfectly plastic-constant porosity version of the Gurson model performed by DRUGAN and MIAO [1992]. Moreover, the results qualitatively agree with the responses of the pressure-sensitive

Table 6. Values of s, ϑ_1, ϑ_2, ϑ_3, and ϑ_4, for $\nu = 1/2$, $\alpha_G = 0.75$, corresponding to different values of porosity Φ, in Mode II plane stress conditions

Φ	s	ϑ_1	ϑ_2	ϑ_3	ϑ_4
0.000	−0.456495	45.807	101.609	132.826	180.000
0.050	−0.453924	46.092	100.186	132.562	180.000
0.100	−0.451126	46.386	98.759	132.295	180.000
0.150	−0.448071	46.690	97.322	132.024	180.000
0.200	−0.444719	47.005	95.869	131.748	180.000

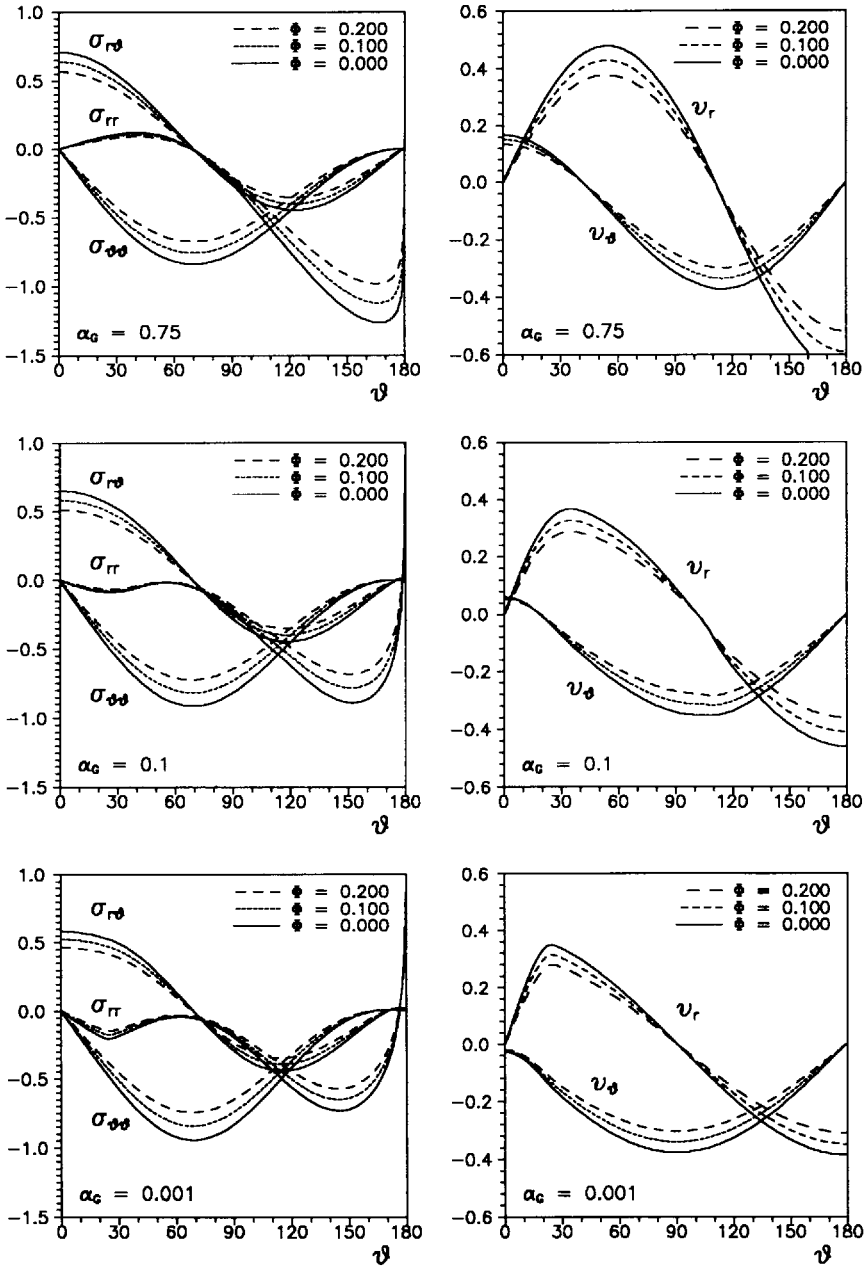

Fig. 13. Angular distribution of stress and velocity functions near crack-tip for various values of hardening of the matrix material (α_G = 0.001, 0.1, 0.75), corresponding to different values of the porosity parameter Φ, in Mode II, plane stress conditions. The case $\phi = 0$ corresponds to the *J_2-flow theory*.

models of HUTCHINSON [1983b], BIGONI and RADI [1993], and RADI and BIGONI [1993]. However, the constitutive laws of the Gurson model, even under the constant porosity assumption, deeply affect the stress state near crack-tip.

The plane-stress and plane strain conditions have been considered. The main conclusions are that high values of the porosity produce:

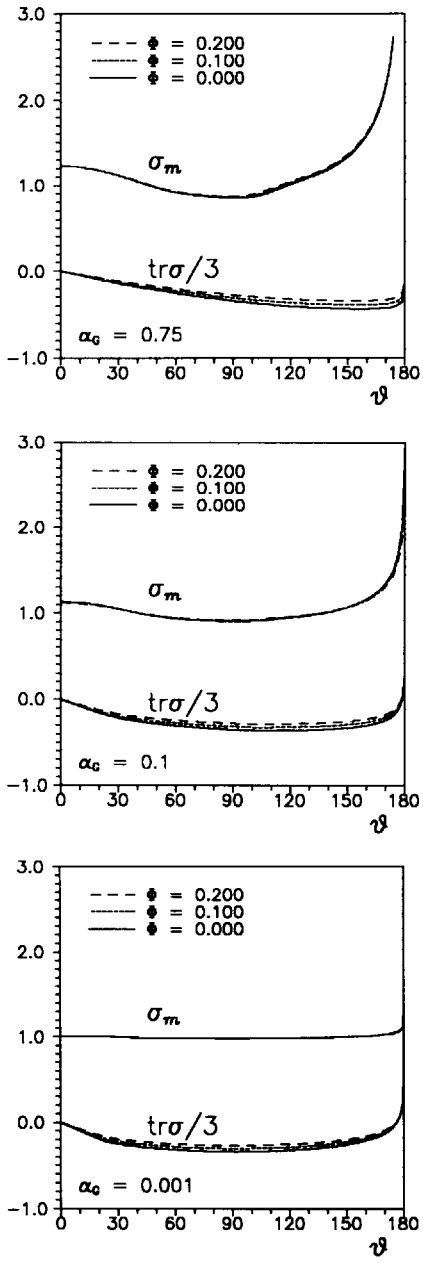

Fig. 14. Angular distribution of mean stress and equivalent stress in the matrix material, for various values of hardening (α_G = 0.001, 0.1, 0.75), corresponding to different values of the porosity parameter Φ, in Mode II, plane stress conditions.

- a lowering in the strength of the singularity
- a reduction of the plastic sectors size
- a concentration of the plastic deformation ahead of the crack-tip
- a lowering in the ratio between the radial and hoop stresses ahead of the crack-tip, related to a decreasing of the mean normal stress ahead of the crack-tip

- a coincidence in the whole plastic sector of the radial stress and the stress component orthogonal to the deformation plane (in plane strain, Mode I loading)
- a change in the shapes of the angular stress distributions, starting from a critical value of porosity (in plane strain, Mode I loading)

The first circumstance suggests that the porosity could have a stabilizing effect on crack propagation. The performed asymptotic analysis proves that continuous solutions for the angular distributions of stresses are possible. However, the above mentioned change in the shape of the stress plots indirectly confirms the validity of the perfectly plastic analysis by DRUGAN and MIAO [1992], where stress jumps have been found.

Moreover, the effects of porosity greatly influence the stress and velocity fields for Mode I loading condition, since the hydrostatic stress reaches high values. In the case of Mode II loading, porosity has small effects on crack-up fields, due to the reduced value of the hydrostatic stress.

Finally, it must be remarked that the solving procedure proposed by PONTE CASTAÑEDA [1987] is very effective in obtaining asymptotic solutions of crack propagation problems even for constitutive laws much more complex than the J_2 flow-theory.

Acknowledgements—The authors thank Prof. Robert H. Dodds, Jr., University of Illinois, Urbana (U.S.A.) for helpful discussions. A grateful acknowledgement is due to the Italian Ministry of University and Scientific and Technological Research (MURST) and to the National Council of Research (CNR Contr.-91.02914.CT07).

REFERENCES

1885 BELTRAMI, E., "Sulle condizioni di resistenza dei corpi elastici," (in Italian) Rend. R. Ist. Lombardo di Scienze, Lettere e Arti, **18**, 704.

1968a HUTCHINSON, J.W., "Singular Behaviour at the End of a Tensile Crack in a Hardening Material," J. Mech. Phys. Solids, **16**, 13.

1968b HUTCHINSON, J.W., "Plastic Stress and Strain Fields at a Crack-Tip," J. Mech. Phys. Solids, **16**, 337.

1968 RICE, J.R., and ROSENGREN, G.F., "Plane Strain Deformation Near a Crack-Tip in a Power-Law Hardening Material," J. Mech. Phys. Solids, **10**, 1.

1975 RUDNICKI, J., and RICE, J.R., "Condition for the Localization of Deformations in Pressure-Sensitive Dilatant Materials," J. Mech. Phys. Solids, **23**, 371.

1977 AMAZIGO, J., and HUTCHINSON, J.W., "Crack-Tip Fields in Steady Crack-Growth With Linear Strain Hardening," J. Mech. Phys. Solids, **25**, 81.

1977a GURSON, A.L., "Porous Rigid-Plastic Materials Containing Rigid Inclusions—Yield Function, Plastic Potential and Void Nucleation," Fracture, 2, ICF4, Waterloo, Canada.

1977b GURSON, A.L., "Continuum Theory of Ductile Rupture by Void Nucleation and Growth: Part I—Yield Criteria and Flow Rules for Porous Ductile Media," Int. J. Engng. Mat. Tech., **99**, 2.

1978 NEEDLEMAN, A., and RICE, J.R., "Limits to Ductility Set by Plastic Flow Localization," in KOISTINEN, D.P., and WANG, N.M. (eds.), Mechanics of Sheet Metal Forming, Plenum Press, New York, pp. 237-267.

1978 YAMAMOTO, H., "Conditions for Shear Localization in the Ductile Fracture of Void-Containing Materials," Int. J. Fracture, **14**, 347.

1981 ACHENBACH, J.D., KANNINIEN, M.F., and POPELAR, C.H., "Crack-Tip Fields for Fast Fracture of an Elastic-Plastic Material," J. Mech. Phys. Solids, **29**, 211.

1981 TVERGAARD, V., "Influence of Voids on Shear Band Instabilities Under Plane Strain Conditions," Int. J. Fracture, **17**, 389.

1982 SAJE, M., PAN, J., and NEEDLEMAN, A., "Void Nucleation Effects on Shear Localization in Porous Plastic Solids," Int. J. Fracture, **19**, 163.

1982 TVERGAARD, V., "Material Failure by Void Coalescence in Localized Shear Band," Int. J. Solids Structures, **18**, 659.

1983a HUTCHINSON, J.W., "Fundamentals of the Phenomenological Theory of Non Linear Fracture Mechanics," J. Appl. Mech., **50**, 1042.

1983b HUTCHINSON, J.W., "Constitutive Behavior and Crack-Tip Fields for Materials Undergoing Creep-Constrained Grain Boundary Cavitation," Acta. Metall., **31**, 1079.

1984 DRUGAN, W.J., and RICE, J.R., "Restrictions on Quasi-Statically Moving Surfaces of Strong Discontinuity in Elastic-Plastic Solid," in DVORAK, G.J., and SHIELD, R.T. (eds.), Mechanics of Material Behavior, Elsevier, Amsterdam, pp. 59–73.
1984 OHNO, N., and HUTCHINSON, J.W., "Plastic Flow Localization Due to Non-Uniform Void Distribution," J. Mech. Phys. Solids, **32**, 63.
1984 TVERGAARD, V., and NEEDLEMAN, A., "Analysis of the Cup-Cone Fracture in a Round Tensile Bar," Acta Metall, **32**, 157.
1985 ARAVAS, N., and MCMEEKING, R.M., "Microvoid Growth and Failure in the Ligament Between a Hole and a Blunt Crack-Tip," Int. J. Fracture, **29**, 21.
1985 MEAR, M.E., and HUTCHINSON, J.W., "Influence of Yield Surface Curvature on Flow Localization in Dilatant Plasticity," Mech. Materials, **4**, 395.
1987 AOKI, S., KISHIMOTO, K., YOSHIDA, T., and SAKATA, M., "A Finite Element Study of the Near Crack Tip Deformation of a Ductile Material Under Mixed Mode Loading," J. Mech. Phys. Solids, **35**, 431.
1987 JAGOTA, A., HUI, C.Y., and DAWSON, P.R., "The Determination of Fracture Toughness for a Porous Elastic-Plastic Solid," Int. J. Fracture, **33**, 111.
1987 NEEDLEMAN, A., and TVERGAARD, V., "An Analysis of Ductile Rupture Modes at a Crack," J. Mech. Phys. Solids, **35**, 151.
1987 PONTE CASTAÑEDA, P., "Asymptotic Fields in Steady Crack Growth With Linear Strain-Hardening," J. Mech. Phys. Solids, **35**, 227.
1987 TVERGAARD, V., "Effects of Yield Surface Curvature and Void Nucleation on Plastic Flow Localization," J. Mech. Phys. Solids, **35**, 43.
1988 ÖSTLUND, S., and GUDMUNDSON, P., "Asymptotic Crack-Tip Fields for Dynamic Fracture of Linear Strain-Hardening Solids," Int. J. Solids Structures, **24**, 1141.
1990 TVERGAARD, V., "Material Failure by Void Growth to Coalescence," Adv. Appl. Mech., **27**, 83.
1991 TVERGAARD, V., and VAN DER GIESSEN, E., "Effect of Plastic Spin on Localization Predictions for a Porous Ductile Material," J. Mech. Phys. Solids, **39**, 763.
1992 AOKI, S., KISHIMOTO, K., and TAKEUCHI, N., "An Elastic-Plastic Finite Element Analysis of a Blunting Interface Crack with Microvoid Damage," Int. J. Fracture, **55**, 363.
1992 DRUGAN, W.J., and MIAO, Y., "Influence of Porosity on Plane Strain Tensile Crack-Tip Stress Fields in Elastic-Plastic Materials: Part I," J. Appl. Mech., **59**, 559.
1992 TVERGAARD, V., and NEEDLEMAN, A., "Effect of Crack Meandering on Dynamic, Ductile Fracture," J. Mech. Phys. Solids, **40**, 447.
1993 BIGONI, D., and RADI, E., "Mode I Crack Propagation in Elastoplastic Pressure-Sensitive Materials," Int. J. Solids Structures, **30**, 899.
1993 RADI, E., and BIGONI, D., "Asymptotic Fields of Mode I Steady-State Crack Propagation in Non-Associative Elastoplastic Solids," Mech Materials, **14**, 239.

Istituto di Scienza delle Costruzioni-Facoltà di Ingegneria
Viale Risorgimento 240136 Bologna, Italy

(*Received in final revised form* 25 *January* 1994)